Overview

Monodisperse magnetic nanoparticles for biodetection, imaging, and drug delivery: a versatile and evolving technology

Shivang R. Dave[1] and Xiaohu Gao[1]*

Advances in nanotechnology have pushed forward the synthesis of a variety of functional nanoparticles (NPs) such as semiconductor quantum dots (QDs), magnetic and metallic NPs. The unique electronic, magnetic, and optical properties exhibited by these nanometer-sized materials have enabled a broad spectrum of biomedical applications. In particular, iron-oxide-based magnetic NPs have proved to be highly versatile deep-tissue imaging agents, having been incorporated into clinical applications due to their biocompatibility. This *Interdisciplinary Review* will focus on the recent advances in strategies for the synthesis and surface modification of highly monodisperse magnetic NPs and their use in imaging, drug delivery, and innovative ultrasensitive bioassays. *WIREs Nanomed Nanobiotechnol* 2009 1 583–609

The most commonly known bulk magnet, iron oxide, is also one of the most commonly employed materials for nanoparticle (NP) synthesis, having a long history of biomedical applications. In contrast to bulk iron oxide, which is a multi-domain ferromagnetic material (exhibits a permanent magnetization in the absence of a magnetic field), iron oxide magnetic NPs smaller than approximately 20–30 nm in size contain a single magnetic domain with a single magnetic moment and exhibit superparamagnetism.[1] The magnetic moment of a particle can rotate through two distinct mechanisms, Néel and Brownian relaxation, thus, over large time scales the net magnetization of a particle averages to zero.[2–6] However, upon application of an external magnetic field, the magnetic moment of the entire particle aligns with the external field yielding a fixed magnetization direction (Figure 1). Of key importance for bioassay applications, superparamagnetic NPs only tend to aggregate due to alignment of magnetic moments in the presence of a strong external magnetic field over long periods of time, whereas ferromagnetic NPs (exhibiting permanent magnetization) are prone to aggregation even in the absence of an external magnetic field. Although larger ferromagnetic particles can exhibit stronger magnetic characteristics due to their larger size, the tendency for aggregation represents a significant drawback for many detection and imaging applications such as magnetic relaxation switching (MRS), which depends upon the relaxivity differences distinguishing single magnetic NPs from their aggregates, and *in vivo* imaging, where the biodistribution profiles of magnetic probes vary drastically depending on size (see below). Owing to their relatively small size, on the order of larger biomolecules or protein complexes, superparamagnetic NPs have greater surface area-to-volume ratios and smaller size than their larger ferromagnetic counterparts, which improves their binding kinetics and biodistribution for *in vitro* assays and *in vivo* imaging, respectively. Consequently, superparamagnetic NPs are ideal for many detection, imaging and drug delivery applications, and will be the main focus of this review.

The most commonly utilized forms of superparamagnetic iron oxide magnetic NPs (SPIOs) in biomedical applications are γ-Fe_2O_3 (maghemite) and Fe_3O_4 (magnetite). Magnetite particles can be converted to maghemite by chemical oxidation, which results in a color change from black to red–brown and a slightly decreased saturation magnetization (M_{sat}). As SPIOs are biologically well-tolerated and of similar

*Correspondence to: xgao@u.washington.edu

[1]Department of Bioengineering, University of Washington, 1705 NE Pacific Street, Seattle, WA 98195, USA

DOI: 10.1002/wnan.051

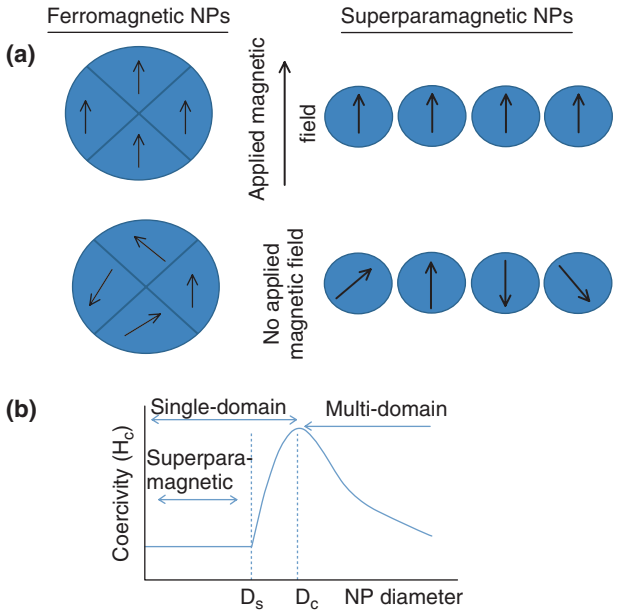

FIGURE 1 | Magnetization behavior of ferromagnetic and superparamagnetic NPs under an external magnetic field. (a) Under an external magnetic field, domains of a ferromagnetic NP align with the applied field. The magnetic moment of single-domain superparamagnetic NPs aligns with the applied field. In the absence of an external field, ferromagnetic NPs will maintain a net magnetization, whereas superparamagnetic NPs will exhibit no net magnetization due to rapid reversal of magnetic moment. (b) Relationship between NP size and the magnetic domain structures. D_s and D_c are the 'superparamagnetism' and 'critical' size thresholds.

size as biomacromolecules, they are ideal scaffolds to be functionalized with biomolecules to produce nanobioconjugates for molecular diagnostics, therapeutics, bioanalytical sciences, and bioengineering.[7–9] Indeed, magnetic NPs conjugated to peptides, antibodies, and nucleic acids have been utilized as contrast agents for *in vivo* magnetic resonance imaging (MRI), as carriers for drug and gene delivery, as cancer therapeutic agents via hyperthermia treatments and as structural scaffolds for tissue engineering.[10–16]

MAGNETIC NP BIOCOMPATIBILITY

A key advantage of iron oxide NPs in comparison to other heavy metal-based NPs for clinical applications is their natural integration into tissue physiology. Iron and its oxides are metabolized, stored and transported through human tissues by proteins including ferritin, transferritin, hemosiderin, and others, such that the resultant iron is incorporated into the iron pool. Administration of 100 mg Fe/kg in rodent models elicited no identifiable side effects, and dose increase to 600 mg Fe/kg did not induce subject death.[17] In typical MRI procedures, the injected dosages of iron oxide contrast enhancement agents are substantially lower than these thresholds.

The native assimilation of iron into the body could potentially improve the compatibility of MRI contrast agents. The widely employed class of chelated Gadolinium (Gd) contrast agents are specifically designed for quick elimination from the vasculature and excretion through urinary tract in order to reduce long-term toxicity. However, in patients suffering from renal insufficiency, associations between the use of such chelates and onset of nephrogenic systemic fibrosis (NSF) and nephrogenic fibrosing dermopathy (NFD) have been well documented. In response, in 2006 the US Food and Drug Administration (FDA) issued a warning with regard to these potential health risks.[18] It is believed that a possible explanation includes the dissociation of the paramagnetic ion from its chelated structure leading to long-term exposure due to the Gd deposited in the body.[19–21]

Although NPs composed of iron oxide are overall well-tolerated *in vivo*, the differences in size, composition, and surface coatings can impact physiological response. Two iron oxide MRI contrast agents used clinically, Combidex® (Advanced Magnetics, employed to differentiate between cancerous and normal lymph nodes) and Feridex® (Advanced Magnetics, employed to detect and evaluate liver lessions) are physiologically benign, but have significantly different degradation profiles *in vivo*. Within 3 days post-injection (intracerebral inoculation or intraarterially after osmotic blood–brain barrier disruption), Combidex® breaks down in the intracranial tissue and after 1 week becomes undetectable, whereas 4 weeks after administration, Feridex® continues to remain visible by MR imaging.[22] In contrast, MION-46 (monocrystalline iron oxide NP) employed in the same study was demonstrated to induce seizures in rats and may not readily degrade in the brain due to a lack of response from local macrophages and reactive astrocytes. In light of these findings, it appears that not only the chemical composition, but the physical size and surface chemistry are important factors in determining biodistribution and physiological response from the host.

The reticuloendothelial system (RES), comprised of the cells in the spleen, liver, and lymphatic system, acts as a defensive mechanism to remove foreign bodies and particulates from the blood stream. Moghimi summarized that NPs should typically be between 120 and 200 nm to avoid sequestration and extravasation to the tissues in order to maximize confinement to the vasculature.[23] Non-specific protein binding to NP surfaces can lead to changes in

overall size and consequent uptake of NPs by the RES system. This represents a significant hurdle to bypass for *in vivo* studies because of significant sequestration and loss of NPs. The standard strategy toward evading RES detection involves the use of non-fouling coatings such as poly(ethyleneglycol) (PEG) and dextran (polysaccharide) to produce 'stealth-like' particles with reduced non-specific binding of plasma proteins and improved circulation half-lives. For instance, Weissleder et al. have used dextran coatings for this reason and have observed blood half-lives of greater than 24 h in humans.[24] An alternative approach has applied zwitterionic surface coatings to NPs (small molecule ligands) and has demonstrated a greatly improved ability to avoid non-specific plasma protein adsorption and RES sequestration.[25] Furthermore, this study illustrated that by successfully avoiding RES sequestration, NPs with hydrodynamic radius smaller than 5.5 nm were able to be eliminated from the body through the urinary tract. Nonetheless, no perfect solution to avoid the RES system has been found, and thus, this area remains highly investigated. It is likely that future solutions to the RES problem will involve the surface engineering of compact NPs such that they appear to be 'natural' to the body. This may be possible by developing NP surfaces that mimick natural biomolecules such as lipids, glycoproteins, and glycogens.

SUPERPARAMAGNETIC NP SYNTHESIS

The synthesis of iron oxide NPs has been an area of intense investigation by chemists and materials scientists for nearly the last half a century. Early investigations have developed a number of methods, such as physical mechanogrinding, gas phase vapor deposition, and aqueous-solution-based routes including microemulsion, sol–gel process, and coprecipitation of ferrous and ferric salts. Breakthroughs in the synthesis of highly uniform semiconductor quantum dots (QDs) in the mid-1990s (involving high-temperature organometallic routes)[26,27] opened up new efficient synthetic routes to produce monodisperse[28] magnetic NPs. The advances in the organometallic synthetic routes have enabled greater control over magnetic NP characteristics and thus revealed new applications arising from the well-defined unique physical and chemical properties.

Traditional SPIO Synthesis

For biomedical applications the two most common aqueous syntheses of SPIOs are alkaline coprecipitation and microemulsion-based precipitation/oxidation of ferrous and ferric salts (Fe^{+2} and Fe^{+3}). Although coprecipitation techniques date back several decades earlier than microemulsion methods, both have continually been refined to yield small magnetic cores typically less than 20 nm. However, the synthesis of small monodisperse NPs is hindered by the inability to precisely control the core size. This is further compounded by the use of surface coatings which introduce large hydrodynamic size variability.

Its long history and synthetic ease have made coprecipitation a common synthetic route. Briefly, iron salts are coprecipitated under aqueous conditions with a strong base to yield the SPIO core which can be either complexed with surface coatings in a one-pot fashion or after purification and dispersion in a multi-step procedure. Common surface coatings include phospholipids,[30] polysaccharides such as dextran, which can be further cross-linked on the surface of magnetic NPs to produce cross-linked iron oxide (CLIO), and polymers such as PEG, polyvinyl alcohol (PVA), and poly-lactic-co-glycolic acid (PLGAs),[31] which can be non-specifically adsorbed or grafted onto the NP surface to produce biomedically relevant aqueous-based SPIOs. A moderate level of synthetic control over NP size and magnetic quality have been achieved through manipulation of factors including solution ionic strength, pH values, and reactant stoichiometries.[32]

A relatively more recent route to SPIO synthesis involves the base-induced precipitation and oxidation of iron salt–surfactant complexes within the cores of nanoscale emulsions. Although this route is generally more controlled with respect to size distribution compared with the coprecipitation method for sub-10-nm particles, only a modest degree of control over particle size and shape can be achieved by controlling reactant stoichiometry, solvent systems, and surfactants—all of which influence the complex dynamics[33] of particle formation. Furthermore, such NPs (particularly larger NPs) suffer from poor crystallinity[34] which can sometimes be remedied through annealing.[35] Recently, Hyeon and coworkers reported a gram-scale SPIO synthesis for generation of highly uniform and crystalline NPs from inexpensive and nontoxic precursors by employing the microemulsion route at elevated temperatures (relative to other microemulsion techniques).[36] NP size ranging from 2 to 10 nm was demonstrated and controlled by precursor and surfactant ratios during the microemulsion procedure wherein reverse-micelles are generated and stabilized at 90°C to promote the reaction. This procedure was extended to produce Mn-, Co-, Ni- and $ZnFe_2O_4$ magnetic NPs.

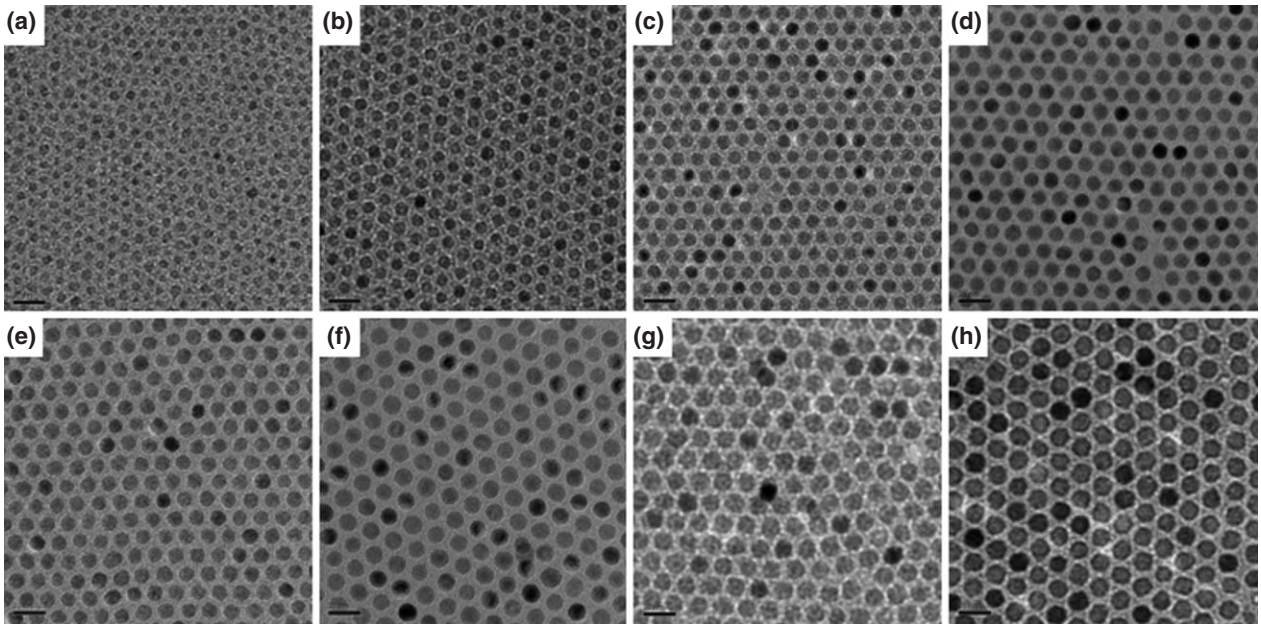

FIGURE 2 | TEM micrographs of iron oxide NPs with diameters of (a) 6 nm, (b) 7 nm, (c) 8 nm, (d) 9 nm, (e) 10 nm, (f) 11 nm, (g) 12 nm, (h) 13 nm. The organic phase high-temperature synthetic route enables precise control of NP size.[29] (Reprinted with permission from Wiley-VCH Verlag GmbH & Co. KGaA).

Although it is difficult to achieve control of NP size with nanometer precision and crystallinity with high fidelity via the techniques discussed above,[37] aqueous synthesis-based SPIOs have been extensively used as MRI contrast agents, bioseparation agents, drug delivery vectors, and other biomedical tools.[32] Despite these achievements, it should be noted that the polydispersity and overall lowered magnetization attributed to the large hydrodynamic size and small core may preclude such NPs from being used in certain biomedical assays which necessitate NP uniformity or thin surface coating. For example, assays that are highly sensitive to NP physical characteristics (such as magnetic moment which depends on core volume and hydrodynamic size which is influenced by surface coatings) include Brownian relaxation-based immunoassays,[2,4,38–40] on-chip separations,[41] biochemical assays,[42] and magnetoresistance biosensors.[43] Recently, it has been demonstrated that the change in MR contrast due to the presence of highly uniform magnetic NPs with sizes spanning between 4 and 12 nm vary drastically,[44] further emphasizing the importance of monodispersity for ultrasensitive biomedical assays. However, besides the particle core size which directly affects NP magnetization, the overall hydrodynamic size is also a critical factor that affects the particle diffusion, *in vivo* biodistribution, and surface functionalities (e.g., curvature and number of ligands). Using highly uniform SPIOs of the same size range (4–12 nm), Colvin and coworkers showed that magnetite particles respond to magnetic field of low gradient in a size-dependent manner, which presents a new opportunity for simultaneous separation of complex mixtures.[45] Thus, future advancements in the application of NPs to biomedical research will require precise control over NP physical characteristics as the power of nanotechnology is closely tied to size-dependent properties. Therefore, the progress of nanotechnology is dependent on improving synthetic routes for producing highly monodisperse NP samples.

Monodisperse Magnetic NP Synthesis

A significant evolutionary branching point in the control over size and properties of magnetic NPs occurred with movement away from low-temperature hydrolytic synthesis techniques toward organometallic procedures carried out at higher temperatures. Additionally, typical iron–salt precursors were replaced with iron–organic ligand based starting materials. Thermal decomposition of iron pentacarbonyl in a dilute solution of functional polymers in organic solvent at relatively elevated temperatures (~150°C) was employed by Griffiths and coworkers in 1979 to obtain single domain (10–20 nm) and single domain superparamagnetic (<10 nm) colloidal Fe and Fe-oxide.[46] In 1993, Bawendi and coworkers employed metal–alkyl precursors, surface coordinating ligands,

and high-boiling point solvents for the high quality and efficient elevated-temperature organic-phase synthesis of semiconductor nanocrystals.[26,47–51] The high-temperature synthetic strategy for QD synthesis was adapted by Alivisatos and coworkers toward the organic-phase thermolysis of iron cupferron complexes in the presence of coordinating ligands to obtain single-crystal maghemite NPs of approximately 10–15% size distribution.[52] Importantly, these techniques have demonstrated exquisite size control, high monodispersity, and enhanced magnetic properties. This stimulated significant expansion of research on the thermolytic synthesis of magnetic NPs by Peng, Sun, Hyeon, and others. Major improvements by Hyeon et al. utilized iron pentacarbonyl precursors and oleic acid as the surfactant for the synthesis of maghemite NPs,[53] followed by additional optimization wherein the large-scale magnetic NP synthesis with 1-nm size control was demonstrated[29,54] (Figure 2). At this point, the synthesis of uniform magnetic NPs is readily obtainable for sizes ranging from 5 to 30 nm in diameter; however, further improvements are yet to be made for the synthesis of larger magnetic NPs by organometallic routes.

The magnetic properties of magnetic NPs can be engineered by tuning the chemical composition (such as iron, cobalt, magnetite, and iron–platinum)[55–57] and NP structure. Sun et al. first reported the synthesis of Mn and Co doped monodisperse iron oxide NPs with a cubic spinel structure.[58] Utilizing the 'polyol' process wherein 1,2-hexadecanediol was utilized to reduce Pt-$acac_2$, as $Fe(CO)_5$ was decomposed in the presence of oleic acid and oleylamine, produced monodisperse FePt NPs. This procedure exhibits flexibility in the choice of metal precursor, enabling different NP compositions and magnetizations to be synthesized such as Fe_3O_4, $CoFe_2O_4$, and $MnFe_2O_4$, from $Fe(acac)_3$, $Co(acac)_2$, and $Mn(acac)_2$ precursors. When transferred into aqueous buffer and applied to biological imaging, the R2 relaxivity of these $MnFe_2O_4$ particles could be 75% stronger than that of pure iron oxide NPs. Despite this R2 enhancement, MR imaging is not as sensitive as other imaging methods, such as optical imaging and positron emission tomography (PET).[59,60] Combining iron oxide NPs with more sensitive imaging modalities has become a topic of intense research for high-resolution and high-sensitivity imaging. Recent research shows that organometallic magnetic NPs made from FePt can be linked with QDs to generate dual-modality NPs.[61] These systems may offer detailed anatomical and molecular information when used for *in vivo* imaging of living organisms. Alternate particle morphologies[62] that deviate from the classical spherical magnetic NPs have been achieved including elongated Fe-based NPs,[63] Fe nanorods,[64] Co nanorods,[65] Fe nanocubes,[66] Co nanodisks,[28] and NPs with internal structures such as hollow core Fe_3O_4 nanocapsules[67] and core/shell configurations.[68,69] NPs with multiple materials have been synthesized by coating magnetic cores with Au shells[70] which allowed easy biofunctionalization[71] and enhanced photothermal therapy properties.[72,73]

The degree of success of the thermolytic method is attributed to the versatility of the organic solvent at dissolving various precursors and surfactants that aid in controlling nucleation and growth.[74–76] Reproducible large-scale synthesis is readily achievable when parameters such as choice of surfactants and precursors, heating rate, and solvent (boiling point) are carefully controlled. For instance, changing precursor to surfactant ratio and/or solvent boiling point have been shown to tune NP size.[29,53–55] Work by Casula and Alivisatos demonstrates that the nucleation is considerably slower than the subsequent growth of NPs, temporally separating the two phases, indicating that the reaction rate can be controlled by the nucleation rate.[77] A distinct feature of magnetic NP synthesis in comparison to high-quality QD synthesis,[26] however, is the absence of a rapid injection of precursor into the hot reaction solution to yield an instantaneously supersaturated precursor solution. Nonetheless, a systematic study of the reaction kinetics of magnetic NPs by Hyeon et al. has shown that the 'heating up' method follows a similar size distribution control mechanism as the 'hot injection' QD synthesis technique, wherein a sudden burst in nucleation is succeeded by rapid size distribution narrowing and a high growth rate.[78]

SURFACE MODIFICATION

Water Solubilization

Before high-quality magnetic NPs synthesized in organic solvents can be applied toward biological applications, their native hydrophobic surface ligands must be modified in order to solubilize them in aqueous solutions. In this regard, the similarity of magnetic NP surface ligands with those of QDs and gold NPs enables the surface-engineering methods previously developed to be easily adopted for magnetic NPs. In general, there are three routes to modify hydrophobic NPs and render them soluble in aqueous biological buffers, as illustrated in Figure 3.

In the first approach, ligand exchange, the native monolayer of hydrophobic surface ligands is exchanged with ligands containing head groups that

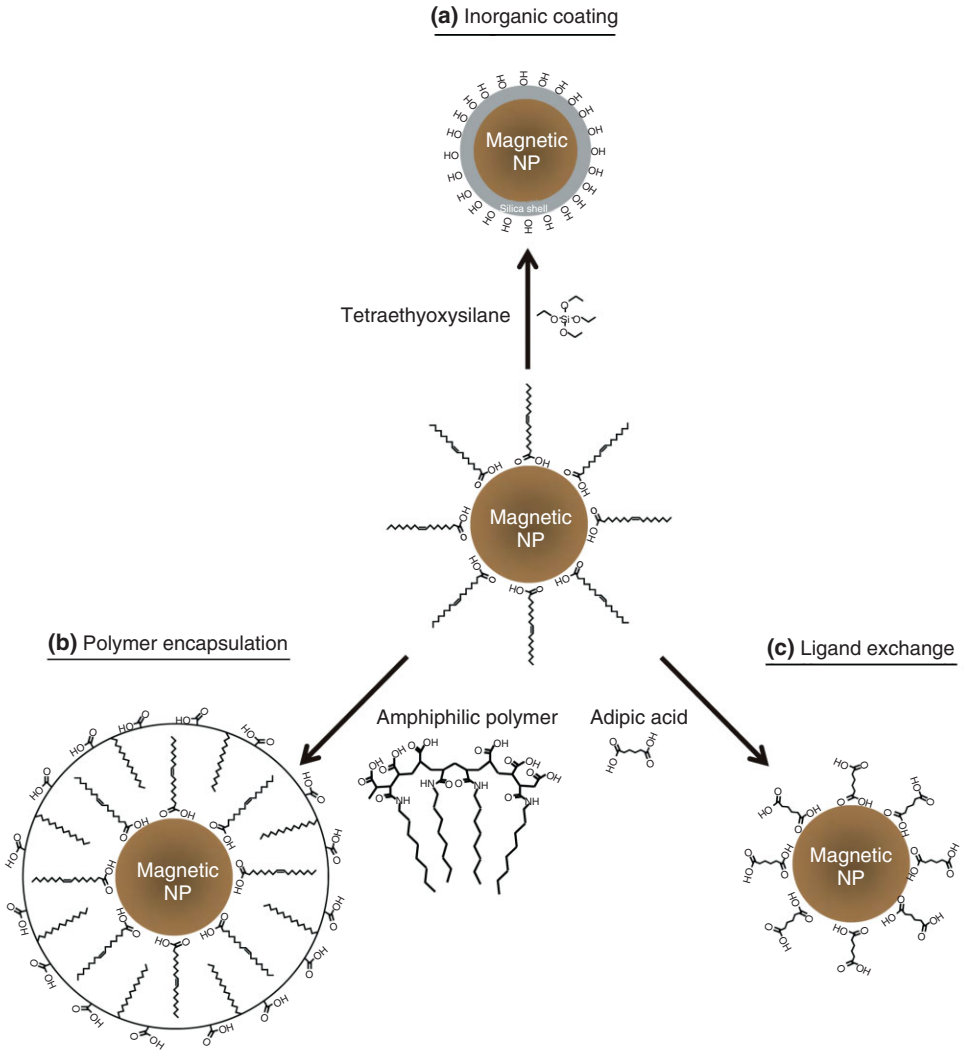

FIGURE 3 | General surface modification schemes for magnetic NPs. (a) Inorganic surface coating with tetraethoxysilane produces an amorphous silica shell. Polymer coating encapsulates the magnetic NP and native surface ligands (b), whereas the ligand exchange is to replace native surface ligands (c). These routes present polar or charged functional groups onto the outer surface of the NP for water solubility.

bind the magnetic NP surface and hydrophilic tails that interact with aqueous solvent.[44] The simplicity of this procedure and wide availability of compatible ligands make ligand exchange one of the most popular and convenient water-solubilization routes.[79] However, a key drawback of this procedure is the potential for desorption of labile ligands from the magnetic NP surface as ligand adsorption is often reversible. Incomplete surface coverage or ligand exchange can result in NP aggregation, inefficient conjugation with biomolecules, and desorption of a bioconjugated surface ligand, all of which can reduce overall biological functionality of the magnetic NP.

In response to the drawbacks mentioned above, an alternative solubilization strategy in which the native hydrophobic ligands are retained on the magnetic NP surface is performed through the adsorption of amphiphilic polymers onto the NP. This general procedure has been used for QD encapsulation with various polymers including octylamine-modified polyacrylic acid,[80] PEG-derivatized phospholipids,[81] block copolymers,[82] and amphiphilic polyanhydrides.[83] As this procedure is general to hydrophobic NPs, it is amenable to hydrophobic magnetic NPs. Additionally, polymer encapsulation with biodegradable amphiphilic polymers originally designed for drug delivery applications[84] can also be applied to further increase the biocompatibility of magnetic NPs particularly for *in vivo* applications since each component of the construct is biocompatible [core material (Fe_3O_4/Fe_2O_3), surface ligands (oleic acid), and polymer coating (polyethylacrylic-polypropylacrylic acid)]. Polymers used for encapsulation contain hydrophobic segments (mostly hydrocarbons) that intercalate and interact with the alkyl tails of the native magnetic NP surface ligands due to the multivalency effect, and hydrophilic segments (PEG or multiple charged groups) which render the overall magnetic NP–polymer constructs soluble in aqueous buffer.

Although there is an increase in the hydrodynamic radius for NPs modified via polymer encapsulation in comparison to the ligand exchange route, the overall NP size is more compact than commonly employed dextran surface coatings for aqueously synthesized SPIOs because the well-defined amphiphilic polymer size and molecular weight result in a monolayer coating. The two general surface modification strategies outlined above present water-solubilizing groups such as carboxyl acids and amines, which in addition to other functional groups, such as azides, are capable of covalent conjugation with appropriate functional groups on the desired biomolecules via standard cross-linking and 'click' chemistries.[85,86] To achieve binding specificity or biomarker targeting abilities, polymer-coated magnetic NPs are generally linked to bioaffinity ligands, such as monoclonal antibodies, peptides, oligonucleotides, or small-molecule inhibitors. Furthermore, conjugation to PEG or similar ligands can improve biocompatibility and reduce nonspecific binding. Due to the large surface-area to volume ratio of magnetic NPs relative to bulk materials, magnetic NPs can be conjugated to multiple molecules to impart multifunctionality and multivalent presentation of affinity ligands to improve target binding.

The third route for magnetic NP surface modification is the fabrication of an inorganic shell, typically consisting of silica or gold, by one of two general schemes: precipitation and reaction at the NP surface[87] or deposition of preformed colloids onto the NP surface.[88] Silica coatings are formed either via the Stöber process[89] or through a microemulsion synthesis. The silica route involves the base-catalyzed hydrolysis of the alkoxides of tetraethoxysilane (TEOS) followed by condensation of the resulting silanol groups. The benefits of silica include its biocompatibility, ease of bioconjugation, and biostability *in vivo*. Xia and coworkers employed a sol–gel approach and demonstrated the direct surface coating of SPIOs with amorphous silica through the hydrolysis and condensation of TEOS with a concentration-dependent shell thickness ranging from 2 to 100 nm.[90] In contrast to previous reports of the *in situ* formation of magnetic NPs and the silica shell, which suffer from poor crystallinity and magnetic properties, Vestal et al. employed a reverse micelle microemulsion scheme with pre-formed high-quality spinel ferrites ($CoFe_2O_4$ and $MnFe_2O_4$) to achieve a silica coating with thickness controlled by reaction time.[91] This technique has been extended to core/shell nanocomposites composed of both magnetic NPs and QDs within nonporous silica coatings, and SPIO/silica core/shell NPs with either non-porous or mesoporous shells.[92,93] In an alternative approach, researchers performed a sol–gel reaction to form mesoporous silica spheres impregnated with monodisperse magnetite and CdSe/ZnS QDs.[94] Hydrophobic nanocrystals were initially transferred into the aqueous phase using cetyltrimethylammonium bromide (CTAB) followed by the subsequent TEOS sol–gel reaction in the presence of ethyl acetate to aid in mesopore formation. The CTAB-coated NPs served as the seeds for silica formation, which resulted in silica spheres with a uniform diameter of ~150 nm and disordered mesopores (~4 nm). Recently, Hyeon and coworkers have demonstrated a one-pot synthesis of discrete uniformly sized superparamagnetic 7-nm core NPs with 5-nm silica shells.[95] A key feature of the reaction is the addition of TEOS to reverse micelles at temperatures low enough to maintain micelle integrity (90°C). Silica shells around magnetic NP cores are important for multifunctional nanomaterials utilized in dual-modal imaging and targeted drug delivery because they enable facile incorporation of fluorescent dyes with the added benefit of increased photostability and intensity due to the 'caging effects'.[96] For instance, Lee and coworkers demonstrated the synthesis of Co ferrite magnetic NPs-silica core/shell NPs incorporating FITC and RITC dyes to provide optical-MR imaging capability in conjunction with PEG and antibodies for enhanced biocompatibility and specific targeting.[97] Thus, silica encapsulation provides a versatile coating capable of increasing NP functionality in addition to rendering hydrophobic NPs water-soluble.

An alternative shell coating is Au, which also has highly desirable characteristics such as biocompatibility, high chemical stability, and ease of biofunctionalization. Direct coating of gold onto magnetic NPs has been challenging due to the differences in crystal properties.[70] In general, synthesis involves the reduction of Au^{3+} ion[98,99] or the deposition of preformed Au NPs[100] onto SPIO cores coated with exposed thiol or amine groups which have affinity for the Au NPs. The reduction of Au ions onto SPIO cores using iterative exposure to hydroxylamine as a reductant[101] or other mild reductants in aqueous micellar medium has been demonstrated,[102,103] but the Au shells are irregular in shape and thickness. O'Connor and coworkers synthesized a 2.5-nm Au shell onto 11-nm Fe core by means of a partial replacement reaction and the subsequent reduction of Au ions onto the core surface.[104] A red-shift in the surface plasmon peak was observed from 520 to 680 nm indicating that an Au shell did form on the Fe core. In another approach, Majetich and colleagues linked discrete Au clusters onto the surface of 12-nm Fe_3O_4 NPs using bidentate

ligands, followed by the electroless deposition of additional gold to complete the shell.[105] While only a rough shell surface was obtainable, the corresponding plasmon peak approached theoretical models of uniform shells. Although breakthroughs have been made, improvements in synthesis are required to obtain highly uniform and reproducible shells.

Bioconjugation

After high-quality NPs have been made water-soluble, bioconjugation to additional biomolecule moieties is performed to incorporate the desired functionality such as targeting ligands (antibodies, aptamers, nucleic acid, etc.), labels (fluorescent dyes or radiolabels), and molecules to improve biocompatibility by reducing non-specific binding (PEG). Several bioconjugation approaches exist including passive adsorption, ligand-mediated linking, and covalent conjugation.

A highly employed modality of passive adsorption is the electrostatic adsorption of highly charged biomolecules such as negatively charged nucleic acid onto a positively charged polymer-coated NP. This approach has been employed for magnetofection applications (see below).[16] Non-electrostatic mediated passive absorption of biomolecules is also possible, for instance, Au NPs and nanoshells are remarkable in their ability to spontaneously chemisorb biomolecules such as antibodies.[106] Thus, Au-coated magnetic NPs are readily amenable to this route. Although passive adsorption is the simplest route to bioconjugation, it suffers from drawbacks including lack of specific orientation of the biomolecule and possibility for biomolecule release due to the non-covalent nature of the interaction.

Ligand-mediated linking shares similarity to passive adsorption in that both persist via non-covalent interactions; however, the former method exhibits more specific control over biomolecule orientation. In general, this system involves an adapter or binding protein and its appropriate ligand. The standard example of this conjugation method is the streptavidin–biotin protein–ligand pair which has been employed to create magnetic NP–biomolecule conjugates.[107] The protein-A/G system specifically binds the F_c region of antibodies and has been widely employed in the assembly of many NP systems since it provides oriented antibody conjugation.[108] An alternate chelation strategy avoiding the use of a binding protein involves the nickel–nitrilotriacetic acid (Ni-NTA) system, which quantitatively binds hexahistidine-tagged biomolecules with precise stiochiometry and molecular orientation. A benefit of this system is the smaller overall size of Ni-NTA and minimization of non-specific interactions with serum proteins in comparison to adapter proteins. Furthermore, the ability to introduce the hexahistidine-tag into the desired location of the desired protein via standard protein-engineering techniques enables potentially better control over biomolecule conjugation and orientation.

The most widely used covalent bioconjugation strategies are carbodiimide-mediated amide formation and succinimide or maleimide-mediated amine or sulfhydryl coupling, respectively. As most biomolecules contain primary amine and carboxylic acid groups, they do not require prior chemical modification before NP conjugation via the carbodiimide chemistry route. Conjugation by means of the activated ester scheme, however, depends upon functional groups not commonly present in biomolecules such as free thiols, succinimide, and maleimide groups. An advantage of this route is specific conjugation to the location where the activated ester species resides, unlike the carbodiimide chemistry which can non-specifically link any primary amines and carboxylic acids. Depending upon the conditions, additional functional groups can be incorporated into the desired biomolecule or NP using reagents that convert primary amines into thiols (Traut's reagent),[109] oxidize diols to yield aldehydes (sodium periodate),[109,110] and introduce alkynes for click-chemistry cycloadditions.[85,86] For instance, pre-activated amphiphilic polymer-containing multiple anhydride rings have been utilized by Pellegrino et al. for NP water-solubilization.[83,111] As anhydride rings are highly reactive toward primary amines, such polymers potentially simplify small molecule conjugation schemes by eliminating the need for coupling reagents.

Although count-less conjugation strategies exist, there is no 'perfect' method to produce NPs with precisely controlled ligand orientations and stiochiometry. These are highly important considerations as these characteristics can greatly impact NP-bioconjugate overall probe size (affecting biodistribution and accessability to intracellular components), synthesis schemes (determining ease of coupling and purification), and ligand density and activity (influencing binding specificity and affinity).

IN VITRO ULTRASENSITIVE AND MULTIPLEXED DETECTION

The primary modality of detection of magnetic NPs is through their effect on MR signal intensity. Magnetic NPs disrupt the magnetic field homogeneity in proximity to their location, thereby altering the

MRI T1 and T2 relaxation times, which results in a contrast enhancement in MR images. The T1 (spin–lattice) and T2 (spin–spin) relaxation times are a measure of the time required to regain longitudinal magnetization following the radiofrequency pulse and the dephasing of coherently 'in-phase' precessing protons, respectively. Magnetic NPs are generally utilized as sensitive negative contrast agents to accelerate the signal decay in a T2-weighted MR image (produce darker or hypo-intense areas), which can be detected using a benchtop relaxometer or MRI instrument.[59]

Magnetic Relaxation Switching

A highly sensitive *in vitro* detection assay was developed by Perez, Josephson, and Weissleder based on the phenomenon that SPIO aggregates more efficiently dephase the spins of surrounding water protons than disperse SPIO NPs (hypothesized to be a function of larger effective cross section).[112] The resulting enhancement of the T2 signal has led to the development of MRS technology for sensitive detection of oligonucleotides,[113] proteins,[114] enzymes,[115] chiral compounds,[116] carbohydrates,[117] and viruses[118] with detection limits as low as 0.5 femtomoles. A key breakthrough of this detection method that bares particular significance for unpurified biological samples is the ability to directly detect magnetic relaxation changes even from opaque samples such as blood and whole-cell lysates which is hard to achieve with many optical detection methods.

In their initial studies, Weissleder and coworkers demonstrated the detection of nucleic acids in solution using two different SPIO populations, each conjugated to oligonucleotide probe sequences complementary to adjacent sites on the nucleic acid target. Hybridization with the target sequence was correlated with a size increase from approximately 50 to 220 nm upon aggregation, which was determined by gel electrophoresis and a reduction in T2 signal from 63 to 45 ms observed within several minutes.[113] In addition to high target specificity, this technology was demonstrated to be hybridization specific since reduced T2 signal was only observed when temperatures were below the melting temperature of oligonucleotide probes. This technology was used to measure telomerase activity and its suppression with small molecule inhibitors in a high-throughput assay format by cycling the reaction to annealing and melting temperatures.[115] This is relevant since elevated telomerase activity is a crucial parameter of genetic instability and malignancy formation. Measurements were performed with a standard benchtop relaxometer and showed that 10–100 attomoles of target could be detected and further confirmed by

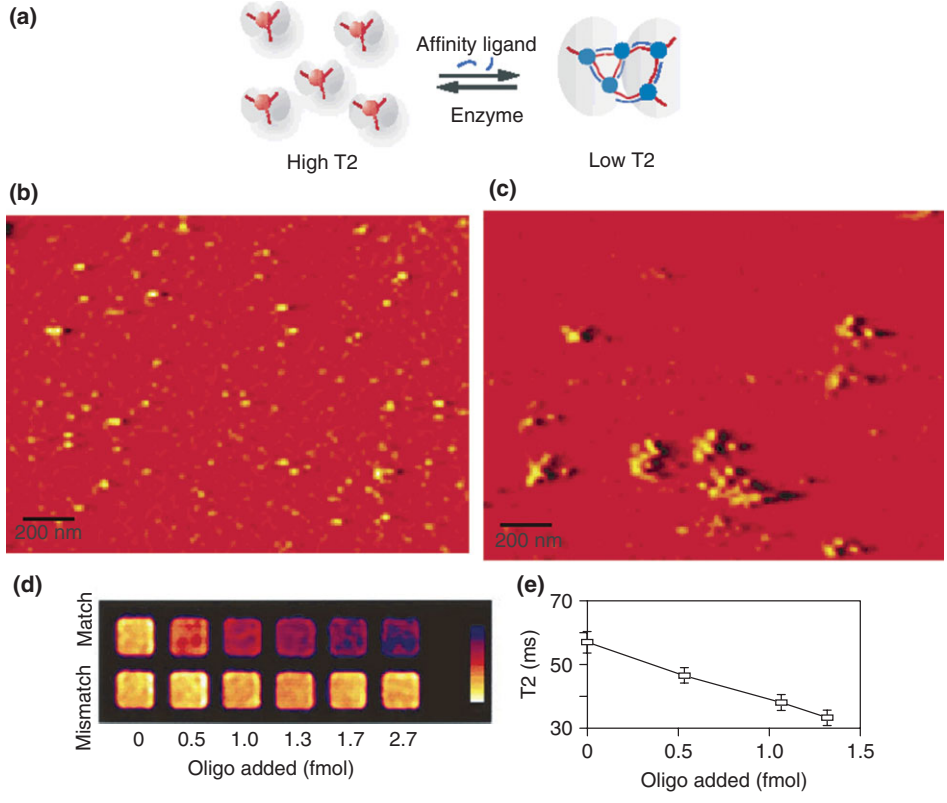

FIGURE 4 | Magnetic relaxation switching technology. (a) Schematic of the transition of dispersed magnetic NPs to nanoclusters with enhanced T2 relaxivity in the presence of ligands such as oligonucleotides. The linker- or ligand-mediated aggregation of nanoclusters can be enzymatically cleaved to yield disperse NPs. (b) AFM image of discrete magnetic NPs. (c) AFM image of nanoclustered magnetic NPs in the presence of target molecule. (d) Nucleic acid detection with MRS. A T2-weighted color-coded MR image of wells of a 384-well plate. Each well contains similar amounts of probes. The concentration of matching and mis-matching target sequence is varied. (e) Decrease in T2 as a function of target sequence concentration, demonstrating detection sensitivity as low as 500 attomoles.[114] (Reprinted with permission from Ref 114. Copyright 2002 Macmillan Publishers Ltd.)

atomic force microscopy (AFM) (Figure 4). Interestingly, screening the reduction in enzyme activity by different telomerase inhibitors in different cell lines indicated the presence of different phosphorylation states of key enzymes among the different cell lines. Further refinement of MRS has permitted the assay of DNA-modifying enzymes such as endonucleases, DNA methyltransferases, and restriction enzymes, which are sensitive to DNA methylation, based on increases in T2 relaxation times resulting from irreversible separation of the appropriate nanoassemblies.[119]

To validate the potential of MRS technology as a diagnostic tool for *in vivo* MR imaging and identification of peroxidase-induced diseases such as atherosclerosis and inflammation, Perez and coworkers modified the assay format to sense for enzymatically catalyzed nanoassembly formation.[120] A benefit of this modification is the potential for extended bioavailability of disperse NP constructs to interact with the targeted blood-pool enzymes and to minimize rapid RES clearance of larger complexed nanoassemblies. Although this system was not applied *in vivo*, disperse serotonin-labeled SPIOs were prepared and were demonstrated *in vitro* to form nanoassemblies catalyzed by the clinically relevant enzyme myeloperoxidase, which is implicated in atherosclerosis.

MRS technology has also been implemented *in vitro* with different modalities of molecular interactions including antibody–antigen in biological samples.[114] SPIO conjugated to virus coat-specific antibodies have enabled the detection of as few as five viral particles per 10 μl for herpes simplex virus-1, while adenovirus was also demonstrated to be detected with this technology.[118] Similarly, the fluorescent protein GFP was detected in cell lysate using antibody-conjugated SPIO via a MRS-based mechanism.[114] A recent report discussed developing SPIO for analyzing the purity of pharmaceutical agents.[116] A model of a toxic enantiomeric impurity, D-phenylalanine (D-Phe), was conjugated to CLIO and mixed with antibody specific to this enantiomer creating crosslinked nanoassemblies with decreased T2 relaxation time. Upon addition of a mixture of free enantiomers, an increase in T2 was observed, indicative of separation of the nanoassemblies due to presence of the enantiomeric impurity. The most recent development in this technology is its application toward continuous glucose monitoring across a semipermeable membrane and the development of SPIO surface-coating libraries sensitive to various analytes.[112,117,121] Importantly, non-invasive continuous sensing of critical targets such as glucose holds promise in the arena of implantable biosensors for the bio-monitoring of diabetes and other diseases.

Magneto-optical Biodetection

Although MRI signaling is a non-multiplexable detection method (or low multiplexing ability), this does not preclude magnetic NPs (or magnetic NP doped microspheres) from utilization in multiplexed assays.[122,123] Recent *in vitro* ultrasensitive detection bioassays integrate magnetic NP-facilitated high-throughput analyte separation with multiplexed optical readout. Among the benefits of this detection scheme are target enrichment from complex biological specimens and multiplexed quantification. Sensitive and specific detection of *E. coli* O157:H7 was demonstrated by Su and Li using QDs as a fluorescence marker coupled with immunomagnetic separation. *E. coli* O157:H7 at a cell concentration of 1000 CFU/ml were detected with an assay time of less than 2 h.[124] To be clinically relevant, magneto-optical-based assays must be capable of target isolation and detection at low concentrations. Unlike nucleic acid targets which can be amplified by polymerase chain reaction (PCR), low-abundance small molecule, carbohydrate, and protein biomolecular targets require signal amplification schemes to increase detection sensitivity. In this regard, Groves et al. detected cytokines at 30 aM concentration[125,126] and Mirkin et al. showed prostate-specific antigen (PSA) detection sensitivity of less than 300 aM.[127] Both detection schemes featured signal amplification and demonstrated the potential for single-molecule detection of genes and proteins. Specifically, Mirkin et al. developed a sandwich assay format utilizing a reporter bead containing tens of thousands of copies of dye-labeled DNA biobarcodes (unique oligonucleotide sequences that 'code for' a given analyte) which act to enhance the signal *in situ*.[127] PSA sandwiched between reporter and magnetic separation beads is magnetically separated and isolated from non-targeted analytes and their respective reporter beads. Afterward, fluorophore-labeled biobarcode DNA sequences are dehybridized from the reporter bead and detected fluorescently (Figure 5(a)). Groves et al. further improved the ultrasensitive biobarcode concept by utilizing magnetic microparticles and porous silica beads containing millions of copies of barcode DNA for the colorimetric detection of ~30 aM cytokine concentration.[125,126] After binding and isolation of interleukin-2, barcode DNA was released from the porous beads. Subsequent hybridization to gold NP capture probes containing complementary oligonucleotide sequences causes barcode-directed clustering of gold NP probes. This solution is spotted onto a thin layer chromatography plate and subsequent detection and quantification

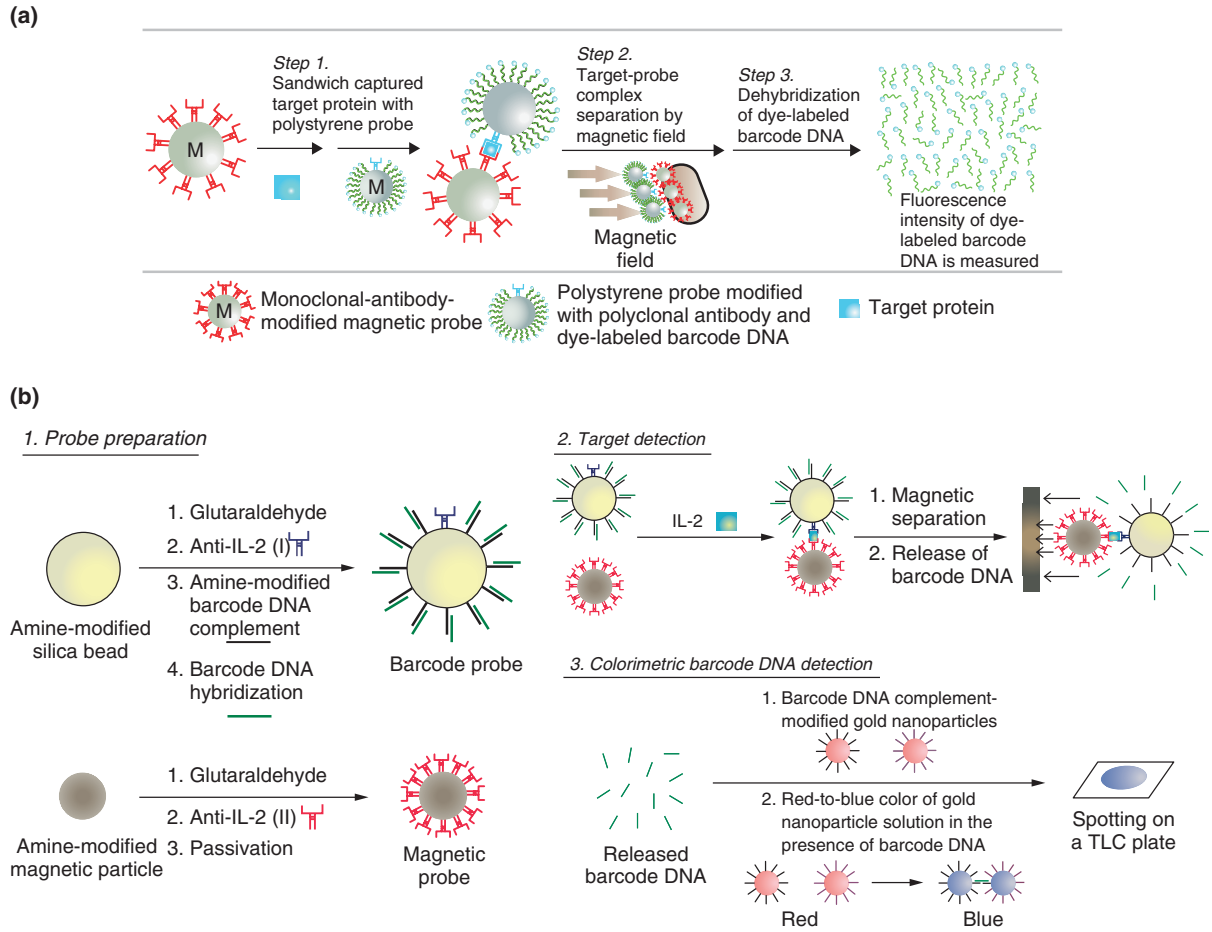

FIGURE 5 | Ultrasensitive detection schemes for assays developed by Mirkin and Groves. (a) Fluorophore-based bio-barcode amplification assay to detect proteins developed by Mirkin.[126] (Reproduced with permission from Wiley-VCH Verlag GmbH & Co. KGaA.) (b) Colorimetric bio-barcode amplification assay to detect cytokines developed by Groves.[127] (Reprinted with permission from Ref 127. Copyright 2007 Macmillan Publishers Ltd). Both assays employ the magnetic NP-loaded microbeads for the separation of positive binding events from the false-positive background in order to increase signal-to-noise ratio. The high sensitivity of these assays is attributed to the high copy-number of dye-labeled barcode DNA and strong optical properties associated with gold NPs, respectively.

of barcode DNA, which is related to target analyte, is determined by the NP cluster-induced red-to-blue color change and spot intensity measurements, respectively (Figure 5(b)). This scheme can be applied toward nucleic acids, small molecules and proteins with potential sensitivity comparable to PCR. In each case, the sandwich assay is based on a pair of molecular probes recognizing distinct domains of target molecules which are conjugated to the magnetic separation bead and optical reporter bead. Only in the presence of the appropriate biomolecular target will both beads be co-localized in the sandwich structure after rapid magnetic separation. In comparison to planar chip-based assays, the significant advantages of homogeneous solution-based assays are faster reaction kinetics[128] and reduced background signal. For instance, target detection and separation via sandwiching by micrometer-sized beads can be accomplished in 1–2 h.[127]

The unique physical properties of magnetic NPs, including MRI contrast and magnetic separation ability, will ensure that they remain an integral part of future bioassays. We envision that future research combining the multiplexing power of optical barcodes and the capability of microfluidic devices to handle small volume samples will lead to detection of multiple biomolecular targets in a single sample with PCR-like sensitivity.

IN VIVO IMAGING WITH MAGNETIC NPs

For deep-tissue imaging, MRI-based detection is one of the most widely used techniques along with

PET in contrast to fluorescence-based modalities, which are limited to imaging depths ranging from millimeters to few centimeters.[12,59] The diagnostic value of MR imaging on patients is improved by the use of a contrast agent in as many as 25% of procedures to extend the capabilities of imaging. The most widely used *in vivo* contrast agents over the last two decades have been chelated paramagnetic ions such as Gd-DTPA, Mn(II)-EDTA, and Cr(III)-EDTA (DTPA is diethylenetriaminepentaacetic acid; EDTA is ethylenediaminetetraacetic acid) which are resolved as bright spots against surrounding tissues as a result of their shortened T1 relaxation times [r1 relaxivities $\sim< 10$ (mM s)$^{-1}$].[129] This class of non-targeted contrast agents was designed to be eliminated from the vasculature and excreted quickly in order to reduce long-term toxicity and not interfere with any future MRI procedures. Although these benefits are necessary, the short retention time limits imaging to a minimal number of scans post injection, which results in poor image contrast enhancement. Furthermore, as each contrast agent molecule typically chelates only one to a few individual transition metals, the magnetic susceptibility is low, which requires large doses to be administered to achieve sufficient contrast enhancement.

In attempts to overcome these limitations, magnetic NPs have become utilized as potentially superior contrast agents. The high magnetic susceptibilities of magnetic NPs locally disturb the magnetic field homogeneity as their magnetic moments align with and enhance the flux of the external magnetic field, resulting in higher relaxivities for magnetic NPs [r1 $\sim$ 3–70 (mM s)$^{-1}$ and r2 $\sim$ 1–650 (mM s)$^{-1}$] relative to chelated paramagnetic ions [r1 $\sim$ 3–6 (mM s)$^{-1}$ and r2 $\sim$ 4–6 (mM s)$^{-1}$].[129–132] Primarily, magnetic NPs (such as iron oxides) are used as T2 contrast agents, although recently developed MnO NPs have been designed specifically for T1 contrast enhancement.[133] Contrast enhancement agents accelerate either the T1 relaxation time (re-alignment of proton spins in the direction of the external magnetic field) or the T2 relaxation time (de-phasing of proton spins) relative to the neighboring tissues, which appear as hyperintense (bright) or hypointense (dark), respectively. The standard field strength for many clinical MRI instruments is 1.5–3 Telsa (T), whereas research and newer instruments employ higher magnetic fields. In general, as field strength increases, signal-to-noise ratio increases which typically facilitates an increase in resolution.[134]

To improve the diagnostic value of MR images, cell- or biomarker-specific contrast enhancement can be achieved with targeted magnetic NPs. In addition to *in vivo* cell recognition, magnetic NPs can be taken up by cells via receptor-mediated endocytosis which is conducive for long-term cell tracking studies.

In vivo Molecular Imaging

Biofunctionalized magnetic NPs have excellent potential to create new *in vivo* imaging opportunities because molecular information, such as the presence and relative abundance of biomarkers, can be assessed by using magnetic NPs functionalized with a myriad of available targeting ligands. Many variations of this concept have been successfully demonstrated with SPIOs synthesized by aqueous routes, including direct cell-surface biomarker tagging,[10] and biotinylated-antibody and streptavidin-coated SPIO two-step labeling.[107] Site-specific accumulation and intracellular uptake of contrast agents are required to generate sufficient contrast enhancement. The transferrin and folate receptors have been extensively used as *in vivo* and *in vitro* targets for transferrin- [135,136] and folate-labeled SPIOs[137,138] to image cancers. Other important biomarkers such as Her-2 (Human Epidermal growth factor Receptor 2, cancer),[107] Annexin V (cellular apoptosis),[139,140] and vascular adhesion molecule 1 (VCAM-1, cardiovascular disease)[141,142] have also been targeted and imaged with hydrolytically synthesized SPIOs.

The new generation monodisperse magnetic NPs have already revealed exciting new discoveries in the field of *in vivo* molecular imaging. This can be attributed to their improved magnetic relaxivities and controlled hydrodynamic size, which translate into increased MR contrast sensitivity and more uniform biodistribution profiles in comparison with the non-optimal physical attributes of hydrolytically synthesized SPIOs. Highly uniform $MnFe_2O_4$ NPs conjugated to anti-Her-2 receptor antibodies were recently developed by Cheon et al.[130] These magnetic NPs with engineered magnetic properties demonstrated approximately four times stronger relaxivity and enhanced contrast ($\Delta T_2 = 34\%$ for $MnFe_2O_4$) in comparison to CLIO ($\Delta T_2 < 5\%$). These enhancements of magnetic properties improve the potential for the sensitive detection of small or early-stage tumors (Figure 6(A)).

In a prior study, the same group utilized 9-nm Fe_3O_4 NPs synthesized via the high-temperature organic-phase route and performed ligand exchange with dimercaptosuccinic acid (DMSA) to yield high-quality water-soluble SPIOs.[143] This ligand presents two distinct advantages. First, the disulfide cross-linking of surface-bound DMSA enhances NP stability in buffered solutions up to 250-mM NaCl and in the pH range between 6 and 10, conditions crucial for biological applications. Second, the small

molecular weight of DMSA (MW = 182) enables NPs to exhibit a smaller hydrodynamic radius than traditional high-molecular-weight dextran systems (MW = 10,000–100,000). For *in vivo* investigations, probe size is a critical factor as biostability, diffusion, nonspecific binding, and RES sequestration can be negatively affected by an increase in size, while tumor penetration depth can be improved by a decrease in size. Utilizing anti-Herceptin antibodies directly conjugated to the magnetic NPs, Cheon and colleagues directly targeted HER2/*neu* receptor (overexpressed in breast cancer cells) *in vivo* using the new generation of magnetic NP probes. Immediately following injection, magnetic NP-Herceptin probes were detected to accumulate *in vivo* at the static tumor site with T2 signal drop of ~10% after 5 min and ~20% after 4 h. Interestingly, at higher magnetic field strengths (9.4 T), the investigators were able to observe the progressive infiltration and targeting of probes into the intratumoral vasculature. It was noted that the time-dependent MR signal change was indicative of the heterogeneous nature of the intratumoral vasculature and delineated the denser tumor core with reduced vasculature from the 'leaky' neovasculatures of the tumor periphery (Figure 6(B)).

Besides tumor imaging, detection and monitoring sites of inflammation and inflammation-specific biomarkers *in vivo* are of substantial diagnostic importance in the clinical setting. Previous studies employing hydrolytically synthesized SPIOs relied on nonspecific uptake of probes by macrophages recruited to the inflammation site. In contrast to such indirect imaging, recent work by Hultman et al. has demonstrated the direct *in vivo* molecular imaging of major histocompatibility complex II (MHC II) expression in the renal medulla using monodisperse SPIO–antibody conjugates.[144] MHC II molecules are transmembrane macromolecular biomarkers of the adaptive immune response and inflammation. To improve *in vivo* plasma lifetime of the hydrophobic 6-nm Fe_2O_3 SPIOs, a PEGylated phospholipid coating was optimized and conjugated to RT1 anti-MHC II antibodies. At 3 T, the r1 and r2 relaxivities were measured to be 25.8 and 266 $\mu M^{-1}s^{-1}$, respectively. It should be noted that these values are substantially higher than the corresponding values for the traditional SPIO ferumoxtran-10 (r1 = 6.58 $mM^{-1}s^{-1}$ and r2 = 127.8 $mM^{-1}s^{-1}$) and Hyeon's similarly sized MnO NPs (r1 = 3 $\mu M^{-1}s^{-1}$ and r2 = 14 $\mu M^{-1}s^{-1}$).[144] The higher relaxivities can be understood in the context of differences in the measurement method, synthesis route, and type of contrast agent. Both Hultman and Hyeon's relaxivity values were reported as a function of magnetic NP concentration, whereas

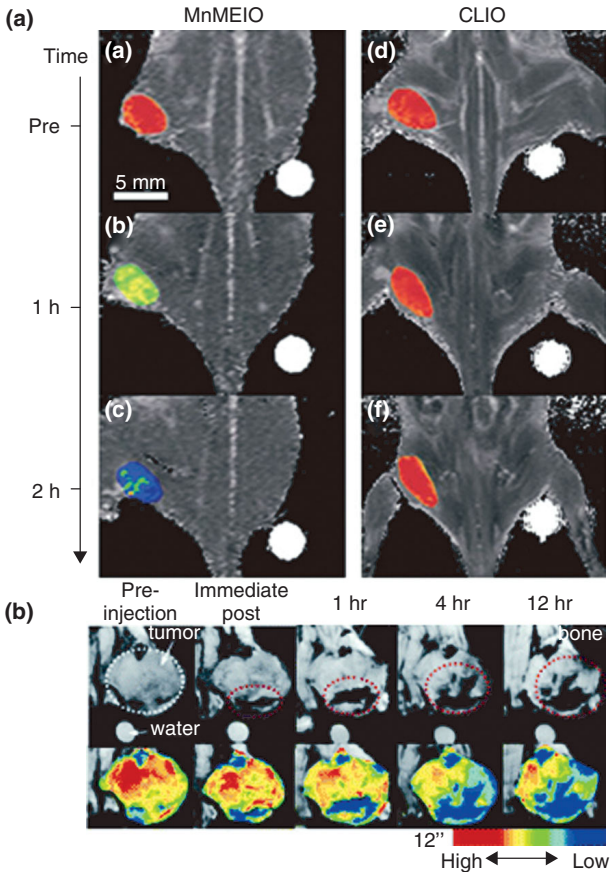

FIGURE 6 | *In vivo* MR detection of cancer using magnetic NP-Herceptin bioconjugates. (A) Color maps of T2-weighted MR images of a mouse implanted with the cancer cell line NIH3T6.7 at different time points after injection of $MnFe_2O_4$–Herceptin conjugates or CLIO–Herceptin conjugates [pre-injection (a,d), 1 h (b,e), or 2 h (c,f) after injection]. In (a–c), gradual color changes at the tumor site, from red (low R2) to blue (high R2), indicate progressive targeting by $MnFe_2O_4$–Herceptin conjugates. In contrast, almost no change was seen in the mouse treated with CLIO–Herceptin conjugates (d–f).[130] (Reprinted with permission from Macmillan Publishers Ltd. Copyright 2006). (B) T2*-weighted *in vivo* MR images of NIH3T6.7 cancer cells implanted in mouse model imaged at 9.4 T. Top panel: Tumor area is circled with white dotted lines, and red dotted lines indicate the hypointense contrast provided by Fe_3O_4 SPIOs. Bottom panel: color-coded MR images to further delineate MR signal changes. The temporal changes in the color maps indicate progressive diffusion and targeting events of the probes (low T2* signal).[143] (Reprinted with permission from Ref 143. Copyright 2005 American Chemical Society.)

the ferumoxtran study normalized the relaxivity values to total iron concentration. Even in light of the fact that an NP contains thousands of atoms, re-normalization of the ferumoxtran relaxivity values with respect to NP concentration would still illustrate improved contrast enhancement of Hultman's magnetic NPs over ferumoxtran. Unlike the aqueous synthesis route for SPIO ferumoxtran, the

organic-phase synthesis of superparamagnetic NPs (T2 negative contrast agent) utilized in this study yields NPs with higher crystallinity. Additionally, Hyeon's MnO magnetic NPs were designed to be used primarily as T1-positive contrast agents, which further explain the difference in relaxivity values. *In vivo* studies performed in rat models indicated a 500% increase in signal half-life at the target site from the specific immunotargeted SPIOs (255 min) in comparison to non-specific controls (45 min). Additionally, R2 values increased from 13 to 22 s^{-1}, from which the researchers were able to calculate a corresponding *in vivo* probe concentration of ~34 nM based on *in vitro* R2 measurements.[144]

In vivo Cell Tracking

Non-invasive cell tracking is desirable for *in vivo* monitoring of administered cell-based therapies in order to elucidate cellular spatiotemporal localization,[145] migration,[146] and dynamics.[147] In line with the great potential represented by stem cells and their therapeutic possibilities, these parameters must be investigated and imaged. Potential stem cell therapies may be used to treat a range of currently irreparable conditions such as spinal cord and myocardium injury, Parkinson's disease, multiple sclerosis, and Huntington's disease by correcting or replacing defective cell populations.[148,149] Additionally, the injection of autologous dendritic or T-cells has been shown to stimulate the immune system to improve various medical conditions including cancer. Dodd et al. utilized MRI and fluorescence colocalization of hydrolytically synthesized SPIO-loaded T cells in tissue phantoms to demonstrate single-cell detection and the potential of SPIOs for cell tracking.[150] Magnetic NPs are ideal candidates for this application due to their biocompatibility and use in MR imaging, which has been shown to achieve whole-body imaging with nearly cellular resolution of 25–50 μm.[146] Along these lines, work involving micron-sized magnetic particles has also demonstrated a similar resolution and the capability for single-cell labeling and detection.[151–153] Although micron-sized magnetic particles exhibit higher relaxivities in comparison to magnetic NPs and have been demonstrated to be uptaken by cells, their extremely large size and non-uniformity are undesirable characteristics for biolabeling. To track cells *in vivo* with MRI, cells must first be labeled with magnetic NPs by one of three general delivery routes[154]: systemic (passive and targeted), *in situ*, or *in vitro*.

After systemic injection of water-soluble SPIOs, non-specific uptake by blood-borne cells such as monocytes and macrophages and subsequent recruitment of these cells to areas of inflammation have been demonstrated.[155] For instance, experimental models of stroke (photothrombosis) in rats have been imaged with this method. Labeled cells, which display hypointense image contrast, were seen to accumulate at the lesion boundary 5-days and infiltrate the lesion core 7-days post-stroke, after an SPIO injection 24 h prior to stroke onset.[156] Immunohistochemical analysis of lesions confirmed the presence of iron-rich macrophages near the lesion boundary.[157] A fundamental concern of relying on passive intracellular labeling via systemic delivery is the increased rate of non-specific labeling of 'off target' cells. In contrast, the targeted labeling of specific cells (as is the case with molecular imaging studies) followed by NP internalization, which often happens through receptor-mediated endocytosis, is a more preferred route.

More directly, SPIOs can be injected into desired tissue with the help of stereotactic imaging equipment. Through non-specific uptake by cells localized to the injection site, NP contrast agents can be incorporated into the desired cells. Shapiro et al. utilized this technique to successfully track the migration of progenitor cells from the subventricular zone to the olfactory bulb, indicative of neurogenesis in the central nervous system (CNS).[158] Although, it should be noted that these studies utilized micron-sized iron oxides, it is expected that high-quality magnetic NPs can improve the detection and tracking sensitivity due to their enhanced magnetic properties. However, the potential for extracellular magnetic NPs to diffuse and provide a background signal at the site of injection is a considerable drawback of this cell tracking method.[154]

Lastly, intracellular labeling of cells *in vitro* and subsequent systemic or site-specific administration is a more precise method to achieve highly specific cell tracking and avoid potential off target labeling.[159,160] In the *in vitro* setting, intracellular labeling with magnetic NPs can be performed in the absence of surface modifications through fluid phase uptake (phagocytosis/pinocytosis)[161] and magnetoelectroporation,[162] or in the presence of surface modifications through the aid of positively charged cell delivery peptides, transfection agents and coatings such as TAT peptide,[163,164] protamine sulfate,[165] and dendrimers,[149] respectively. Positively charged surface coatings promote enhanced interaction with the negatively charged cell membrane.[16] In an early study, Weissleder and coworkers demonstrated that dextran-coated MION could be uptaken into different tumor cell lines via pinocytosis and phagocytosis, with the more phagocytic cell lines incorporating a greater number of NPs.[161] A more general method is electroporation, which can be

utilized to introduce magnetic NPs into the cell without the need of specialized surface modifications. Although this technique can be harmful to cells, optimization of voltage and pulse duration parameters demonstrated picomolar loading of FDA-approved Feridex® into human mesenchymal stem cells and hematopoietic ($CD34^+$) stem cells without noticeable side effects to cells.[162] An alternative approach to efficient cellular uptake[161,162] for cell types that inherently have low non-specific uptake levels[166] is with cell-penetrating peptides (e.g., TAT) that have been highly employed because of their high efficiency. Weissleder and coworkers have observed that TAT-functionalized dextran-coated SPIOs have a significant reduction in blood circulation half-live from approximately 655–47 min and increase in parenchymal intrahepatic distribution of NPs in the liver over unmodified NPs.[167] In another study, TAT-mediated delivery achieved over 100-fold increase in SPIO uptake into hematopoietic and neural progenitor cells (an iron loading content per cell ~10–30 pg) over unmodified NPs.[148] After intravenous injection of labeled cells into immunodeficient mice, single cells could be detected by MRI and recovered using magnetic separation columns from bone marrow samples.[148] Using the transfection agent protamine sulfate, Guzman et al. incorporated Feridex IV (SPIO synthesized via aqueous routes) into human CNS stem-cell-derived Neurosphere cells and demonstrated that the SPIO-labeled stem cells produced normal migration patterns and differentiated into neuronal and glial cells in neonatal, adult and injured NOD-SCID mice according to the respective microenvironmental clues.[168] A dendrimer-coated SPIO formulation, termed 'magnetodendrimers', developed by Bulte et al. was also shown to intracellularly label mammalian stem cells without the need of cell-specific ligands and without affecting cell viability or proliferation. Remarkably, these cells were able to be imaged *in vivo* up to 6 weeks post-transplantation.[149]

Researchers have combined scintigraphic and MR-based cell tracking to gain insights into the clinical study of cell-based therapies. Recently, de Vries et al. demonstrated the tracking of autologous *ex vivo* cultured SPIO-loaded dendritic cells in human clinical trials for melanoma therapy.[169] Antigen-presenting immune cells such as dendritic cells are of immunological importance as they become activated against threats such as cancer. In comparison to scintigraphic imaging of dendritic cells labeled with ^{111}In radioisotopes, co-injected SPIO-loaded cells showed substantially better resolution when observing the drainage of cells from one lymph node to neighboring nodes. Saturation of scintigraphic images was observed, concealing a group of five positive lymph nodes as only four, whereas MR imaging was able to distinguish and reveal all five positive lymph nodes. This study shed light on limited therapeutic responses observed in ongoing clinical trials, as MRI indicated that nearly half of injections were administered to the perinodal fat and not the actual lymph node which gave explanation for low cell migration rates. On the basis of the quantified scintigraphy of a resected lymph node, the researchers were able to conclude from MR imaging of the same lymph node that as few as 1.5×10^5 migrated SPIO-loaded cells could be visualized *in vivo*. Despite the higher spatial resolution of MRI, scintigraphic imaging is still the preferred method to quantify cell migration because of higher sensitivity.

Doped-magnetic nanostructures can be engineered to circumvent the low sensitivity attributed to MR imaging and provide *in vivo* T1 contrast enhancement. Most recently, Dai et al. prepared FeCo/single-graphitic carbon-shell nanocrystals (FeCo/GC) using a chemical vapor deposition method.[131] The particles show outstanding relaxivity values with r1 of 70 $mM^{-1}s^{-1}$ and r2 of 644 $mM^{-1}s^{-1}$, thereby enabling their use as improved T1 and T2 contrast agents. For comparison, the r1 and r2 values of commercially available Feridex® and Magnevist® (gadopentetate dimeglumine, Berlex) are only 10 and 104 $mM^{-1}s^{-1}$, and 4.6 and 4.5 $mM^{-1}s^{-1}$, respectively. The FeCo/GC NPs were readily internalized by mesenchymal stem cells without the need of a delivery agent, and demonstrated significantly higher T2 contrast at lower doses than Feridex-loaded cells *in vitro*. After adsorption of phospholipid-PEG onto the surface, the water soluble FeCo/GC were noted to have a stronger and longer-lasting positive-contrast enhancement (T1) of the blood pool *in vivo* than conventional iron oxide and Gd agents.

Even in light of the benefits and achievements in *in vivo* cell labeling and tracking, Bulte et al. have illustrated the limitations in the applicability of magnetic NP cell labeling for rapidly-proliferating and asymmetrically dividing cells types due to loss of signal and sensitivity.[170] Nonetheless, *in vivo* tracking of magnetically labeled cells is likely to continue to advance as valuable insights have already been afforded with many cell types.

MAGNETIC NPs AS DELIVERY VEHICLES

The dual-functional nature of magnetic NPs as both imaging agent and physical handle for manipulation under a magnetic field gradient has made them

attractive delivery agents *in vitro* and *in vivo*. Due to the potential off-target effects such as non-specific toxicity associated with anti-cancer drugs, targeted delivery is highly desired. The potential for magnetic manipulation of magnetic NPs can be used to attenuate the off-target effects of highly cytotoxic agents when the two are combined.

Small Molecule Drug Delivery

A recent trend for drug delivery applications has been the employment of multifunctional particles containing magnetic NPs to provide imaging functionality, cell-specific targeting, and controlled drug release.[94,171] Although there exists an extensive body of literature on the incorporation of SPIO into microbeads,[122,123] the development of multifunctional nanobeads has only been achieved recently for drug delivery applications. Magnetic NP-based drug delivery vehicles offer MRI contrast enhancement as well as the ability to be guided physically by a magnetic field gradient for enhanced and localized drug delivery.[172–176]

A novel multifunctional polymeric micelle was developed by Nasongkla et al. to specifically target and deliver doxorubicin (DOXO) to cancer cells with up-regulated $\alpha_v\beta_3$ integrin expression via cRGD ligands.[177] By means of a solvent-evaporation method, monodisperse 8-nm SPIOs were co-loaded with DOXO into an amphiphilic block copolymer micelle consisting of maleimide-terminated PEG-block-PLA and methoxy-terminated PEG-block-PLA. The overall size of the multifunctional constructs was approximately 45 nm as confirmed by TEM and dynamic light scattering. Control over maleimide surface density ranging from 0 to 16% of PEG chains was achieved by adjusting the ratio of the two block copolymers. Importantly, pH-dependent release of DOXO was achieved because of the ionizable amine groups in DOXO and the amorphous nature of PLA, such that higher concentrations of DOXO were found in the cell nuclei compared to other studies utilizing more crystalline poly(e-caprolactone). Cytotoxicity occurred in SLK endothelial cells derived from human Kaposi's sarcoma specifically expressing $\alpha_v\beta_3$ integrin. Additionally, SPIO to micelle loading density was as high as 50% by weight, which enabled a significant improvement in the T2 relaxivity allowing for *in vitro* detection of nanomolar concentrations of multifunctional micelles. In cells, micelles with 16% cRGD surface density enhanced the MR image contrast (cells appeared darker due to the accelerated decay of the T2 signal by magnetic NPs) to a greater degree than micelles lacking the targeting ligand. It should be noted that control experiments indicated that at higher micelle concentrations, nonspecific uptake was observed. The presence of 16% cRGD in the micelles had an approximately 2.5-fold increase in cell uptake and 7-fold decrease in cell growth over non-cRGD containing micelles.

Along these lines, Hyeon and coworkers recently designed a multifunctional PLGA nanostructure incorporating 15-nm monodisperse SPIOs for MR imaging, 3-nm QDs for fluorescence visualization, and DOXO as a therapeutic agent.[178] The 100–200 nm multifunctional NPs were formed by an oil-in-water emulsion using a nonionic amphiphilic surfactant under sonication followed by solvent evaporation. For cancer-specific targeting, poly(L-lysine)-poly(ethylene glycol)-folate (PLL-PEG-FOL) ligands were electrostatically adsorbed onto the NPs, which increased the zeta potential from −32 to +22 mV. Nanoconstructs lacking folate ligands and DOXO were shown to have little effect on cell viability, whereas incorporation of both components into the NPs lowered cell viability to approximately 70%. Although the ligand-mediated specificity and therapeutic effect were improved in relation to free DOXO (cell viability ~80%), targeting remained non-optimal which can be reconciled due to electrostatic adsorption of positively charged nanoconstructs to the negatively charged cell membrane. To improve therapeutic efficacy, a synergistic targeting strategy was facilitated by the incorporated SPIOs, wherein the nanoconstructs were manipulated by a magnetic field and concentrated near cancer cells *in vitro*, which correspondingly further decreased cell viability from ~70 to 40% (Figure 7).

Another variation of the multifunctional NP was investigated by Zink and coworkers using mesoporous silica.[179] This work demonstrated the ability to simultaneously image (via fluorescence and MRI) and deliver water-insoluble therapeutics to tumors using multifunctional mesoporous silica-magnetic NP platforms. Hydrophobic 20-nm monodisperse SPIOs were synthesized via high-temperature organic-phase methods and transferred into the aqueous phase with the amphiphilic surfactant CTAB upon evaporation of the organic phase. A 100–200 nm thick mesoporous silica shell was grown around the water-solubilized SPIOs using TEOS within a controlled temperature range (65–80°C). Afterward, FITC dye was conjugated to the pore walls and particle surface to provide fluorescence functionality. To prevent NP aggregation during hydrophobic drug loading, surfaces were modified with trihydroxysilylpropyl methylphosphonate to inhibit interparticle hydrogen-bonding between the surface silanol groups. Using a clinical MRI instrument the aqueous NPs at a

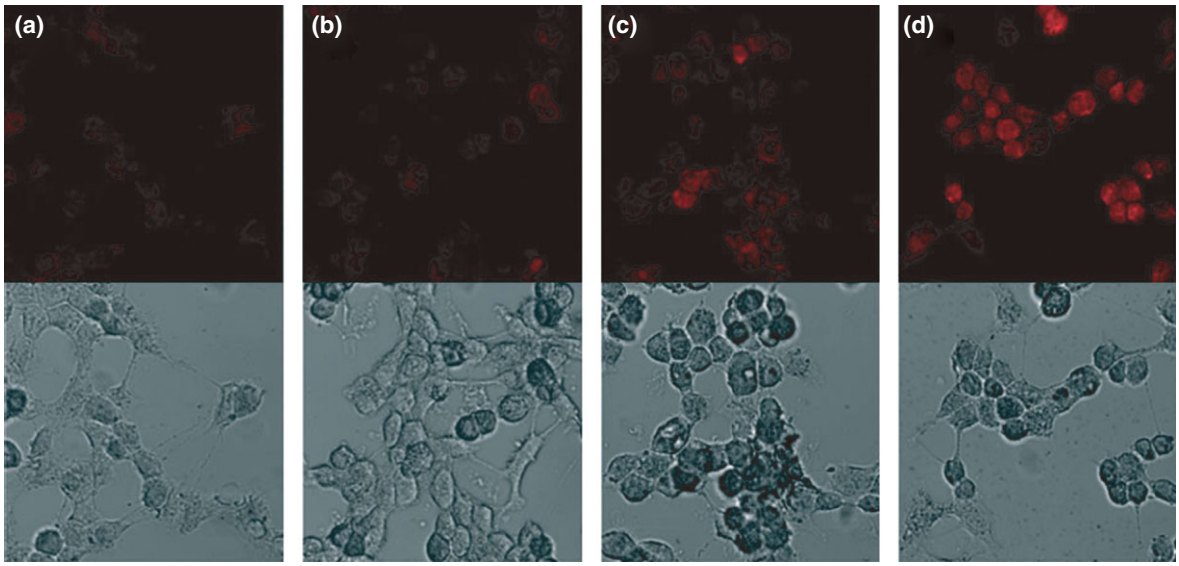

FIGURE 7 | Confocal laser scanning microscopy of DOXO fluorescence and optical images of multifunctional PLGA NPs developed by Hyeon et al. in KB cells treated with: (a) naked PLGA(SPIO/DOXO), (b) PLGA(SPIO/DOXO)-PEG, (c) PLGA(SPIO/DOXO)-Folate NPs and (d) PLGA(SPIO/DOXO)-Folate NPs exposed to an external magnetic field.[178] The fluorescence increase indicates the increase in multifunctional NP uptake mediated by the folate ligand and further uptake enhancement by the presence of an external magnetic field. (Reprinted with permission from Wiley-VCH Verlag GmbH & Co KGaA).

concentration of 1 mg/mL produced hypo-intense (negatively enhanced) T2-weighted MR images. It is likely that such a high NP concentration is needed to achieve MRI contrast enhancement because of the low magnetic NP loading density and the thick silica shell which reduces the interaction between magnetic NPs and water molecules. To demonstrate drug loading and deliverability, the water-insoluble anti-cancer drugs camptothecin (CPT) and paclitaxel (TXL) were utilized. UV/vis spectroscopy indicated 4% of the stored drug leached out in aqueous solution after 6 h, whereas all of the stored drug (~30 nmol per 1 mg silica NPs) were released in DMSO or methanol, suggesting slow release kinetics could be achieved *in vivo*. Cytotoxicity and targeted delivery were studied using pancreatic cancer cell lines PANC-1 and BxPC3, which indicated that the observed cytotoxicity was attributed to the drugs and not the silica NPs for the concentrations used. In this study, folic acid was chosen as a targeting ligand due to the over-expression of folate receptor in PANC-1 and not human foreskin fibroblast (HFF) cancer cell lines. A two-fold increase in NP uptake was observed in PANC-1 cells due to folate modification and not in HFF, although both cell lines exhibited baseline levels of NP uptake. Cytotoxicity studies illustrated the receptor-dependent cytotoxicity effect; HFF cells treated with NPs with and without folate had similar cell survival, whereas PANC-1 cells demonstrated increased cytotoxicity with folate modified NPs. It is likely that increased magnetic NP loading density can also improve MRI sensitivity of these silica NPs.

Nucleic Acid Delivery

The highly efficient delivery of nucleic acid cargo, such as anti-sense oligonucleotides, siRNA (small interfering RNA) and plasmid DNA (pDNA), has been an important milestone for researchers in molecular biology, gene therapy, and clinical arenas. Viruses are nature's most efficient nucleic acid delivery vehicle, yet, the use of viral vectors (e.g., adeno- and retrovirus) in gene therapy is limited by inherent possible health risks such as the potential for immunogenicity and insertional mutagenesis.[16] In light of such potential difficulties, biocompatible magnetic NPs[180] have been investigated as alternative non-viral delivery vehicles utilized as either magnetically responsive or as passive delivery vehicles.

The *in vitro* or *in vivo* magnetic NP-aided delivery of therapeutic or reporter genetic material to cells under the direction of external magnetic fields has been termed 'magnetofection'[16,180,181] (for a historical account of the development of magnetofection see Mykhaylyk et al.[181]). Typically, genetic material is physically adsorbed or chemically conjugated to a magnetic carrier which is encapsulated with transfection enhancing polymers such as PEI (a cationic polymer known to increase nucleic acid

adsorption, cell surface association, and endosomal escape). The driving force for *in vitro* magnetofection is the magnetic field gradient across the cell, creating a physical force on magnetically responsive NPs, thereby eliminating the normally diffusion-limited localization of gene delivery agents to the cells.[182] The resulting decrease in the sedimentation time (on the order of minutes) enables nearly the entire applied dose to reach its cellular targets, yielding an improvement in the net transfection efficiency by several orders of magnitude.[16,183] A reduction in toxicity[184] is observed due to the minimization of applied dose, incubation time, and exposure to cationic transfection agents which exhibit varying levels of cytotoxicity.

Breakthroughs by Plank et al. elevated the power of magnetofection using hydrolytically synthesized magnetic NPs by demonstrating therapeutic magnetofection in primary cells (non-immortalized cells freshly isolated from an organism). Initial efforts demonstrated a significant reduction in *in vitro* transfection time while maintaining overall transfection levels when compared to lipid-based transfection agents. The cell lines this technology has been applied to *in vitro* include lung epithelial,[185] blood vessel endothelial,[186] primary human cells (including keratinocytes, chondrocytes, osteoblasts, and aminocytes),[16] and whole-tissue specimens of airways and blood vessels. In blood vessel endothelial cells, Krotz et al demonstrated the delivery of synthetic antisense oligonucleotides to inhibit the expression of target genes through the delivery of siRNA for the knock-down[16,184] of luciferase reporter gene expression in HeLa cells. This body of work illustrates the efficient nucleic acid delivery potential of magnetofection, establishing it as both a molecular biology research tool and a therapeutic tool.

Compared to *in vitro* targeting and transfection, magnetofection *in vivo* is more difficult to achieve. Nonetheless, Plank and coworkers successfully demonstrated site-directed vascular delivery using magnetic fields with high levels of gene knockdown after injecting antisense oligonucleotide-SPIO complexes into the femoral arteries of mice. The application of the magnetic field localized those constructs to vascular tissue, but not on the contralateral tissue where no field was applied.[184] The same group demonstrated that PEI-SPIO complexed with gene vectors could be targeted under the influence of external magnetic fields and withstand the harsh physiological conditions (extreme pH, abundance of degradative enzymes, etc) of the ilea lumens of rats, or stomach lumens of mice. The application of a magnet to the intestinal area produced efficient and abundant transfection when compared to viral and no-magnet controls.[187] In both studies, magnetic vector targeting permitted the use of reduced dosages and shorter incubation times while improving *in vivo* transfection efficiency.

Despite these positive initial findings, challenges remain for *in vivo* magnetofection as illustrated by Xenariou et al. in their attempt to produce efficient magnetofection *in vivo* using the mouse nose as a model for airway gene transfer.[188] Even after significant optimization of their PEI-SPIO-pDNA complex, the addition of the magnetic field produced no significant enhancement in transfection efficiency, which the authors attributed to the mucociliary barriers to entry.

A new approach to this problem has been reported by Rudolph and colleagues involving 'nanomagnetosols' (SPIOs aerosolized into droplets) guided by external magnetic fields.[189] After theoretically demonstrating feasibility through computational simulation, targeted aerosol delivery to mouse lung was achieved. Aerosol droplets of mean diameter 3.5 μm containing approximately 2930 SPIO NPs were delivered by intratracheal intubation. Application of an electromagnet tip to the right lung lobe increased SPIO deposition by eightfold relative to the left lung, whereas even amounts were distributed to both lungs when no magnetic field was applied. Histological assessments indicated higher concentration of SPIOs in the epithelial cells near the magnet and homogeneous distribution in the opposite lung lobe. For targeted therapeutic delivery, pDNA-SPIO co-formulated nanomagnetosols were also shown to have a twofold increase in delivery in the presence of a magnetic field. An advantage of this approach is that the nanomagnetosol droplet acts as the drug delivery vehicle so the drug does not need to be conjugated to the NP. Additionally, this formulation strategy does not require the SPIOs to be retained at the delivery site, as unbound drug is free to diffuse through the mucous layer, providing flexibility in choice of drug and NPs incorporated into the aerosols. As the magnetic field gradient diminishes rapidly with distance, challenges remain in scaling up the magnetic field gradient to the necessary strengths required for human lungs. Nonetheless, progress with multimagnet designs and high field gradient electromagnets will likely improve the feasibility of this technology for larger mammals.

Non-magnetically guided delivery of siRNA to achieve *in vivo* gene silencing in tumors combined with both MR and optical imaging using dextran-coated SPIO probes conjugated to myristoylated polyarginine peptide (MPAP) was performed by Medarova et al.[190]

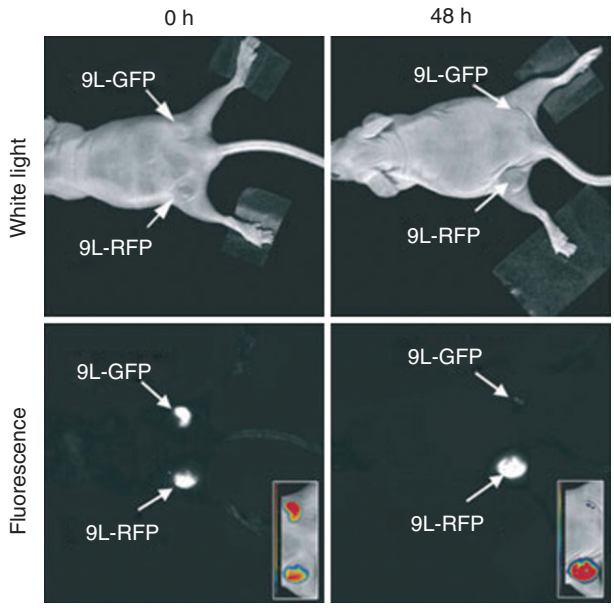

FIGURE 8 | *In vivo* near-infrared optical imaging of SPIO-siGFP constructs and effects on gene silencing in tumors. Mice with bilateral 9L-GFP and 9L-RFP tumors are imaged before and 48 h after intravenous probe injection. Substantial decrease in 9L-GFP-associated fluorescence was observed, in contrast to 9L-RFP (no change). GFP and RFP images were acquired individually and later merged.[190] (Reprinted with permission from Ref 190. Copyright 2007 Macmillan Publishers Ltd.)

As a proof of concept, the siGFP-SPIO probes achieved gene-specific silencing of GFP in mice with bilaterally implanted 9L-GFP and 9L-RFP tumors as indicated by a decrease in the GFP signal in contrast to no change in the RFP signal, detected by *in vivo* optical imaging (Figure 8). The 9L gliosarcoma cell lines have been engineered to constitutively express either humanized GFP or RFP so that they can be visualized without the need for additional histological staining.[191] Tumor T2 signal was also noted to decrease upon administration of the SPIO probes which further confirmed probe accumulation at the tumor site. Quantitative RT-PCR analysis established that the probes reduced GFP mRNA levels in comparison to saline- and mismatch-treated controls by 85 and 97%, respectively. A key aspect of this work was the application of these probes in a therapeutic scenario. The NP probes were modified to target and silence the anti-apoptotic gene *Birc5*, a therapeutic target with restricted expression in tumors. Magnetic-siRNA probes were systemically delivered four times in 2 weeks to nude mice bearing subcutaneous human colorectal carcinoma tumors. Again, MRI and near-infrared optical imaging illustrated NP uptake into the tumor in accordance with the 'enhanced permeability and retention' (EPR) effect observed in tumors even though the probes were not conjugated to tumor-targeting ligands. Notably, an increase in tumor apoptosis and necrosis was observed in comparison to controls and was further corroborated by a decrease in mRNA transcript levels for SPIO-siRNA probe treatments by 97 and 83% with respect to blank SPIO and SPIO-mismatch siRNA probe groups. The SPIO carrier preserved siRNA biological activity and enhanced siRNA stability and biodistribution, which in conjunction with MPAP for ligand-mediated membrane translocation and cytoplasmic localization, produced substantial gene silencing in tumors.

SUMMARY AND PERSPECTIVE

Magnetic NPs represent a versatile class of materials with numerous applications arising from their physical properties. Until recent breakthroughs in synthesis of monodisperse high-quality magnetic NPs, their application had been limited. Further improvement of the magnetic properties of NPs via new compositions and structures will likely improve relaxivities and consequently increase sensitivity in down-stream applications. Since the hydrodynamic size and surface characteristics are important for many *in vitro* and *in vivo* applications, future improvements, such as the employment of non-fouling zwitterionic surfaces and bioconjugation strategies that enable facile covalent linking of biomolecules with precise orientation and stiochiometry, will remain the areas of interest. As the field realizes the growing importance of the benefits provided by newer magnetic NPs, it is expected that magnetic NP-based technologies will become broadly utilized in biomedical applications. Indeed, magnetic NP-based constructs have been demonstrated to improve *in vitro* biodetection sensitivity, increase *in vivo* molecular imaging capability, and enhance drug delivery efficiency. Over the next couple of years, multifunctional NP-based systems will continue to mature and incorporate further functionality, heightening their impact upon deep-tissue imaging, ultra-sensitive biomarker detection, and on-demand *in vivo* drug release. The potential for advancements in clinical detection, diagnosis, and prognosis of complex diseases such as cancer, cardiovascular and neurological disorders, and their therapeutic intervention are on the horizon. Monodisperse magnetic NPs hold promise to enable new applications, such as cell membrane manipulation and signal transduction actuation[192] for fundamental biological investigations, highly sensitive spintronics-based detection technologies for molecular sensing,[193,194] and the clinical application of multifunctional nanomedicine platforms.[195]

ACKNOWLEDGEMENTS

X.G. thanks Department of Bioengineering at the University of Washington for the new faculty startup fund and the National Science Foundation for a Faculty Early Career Development award (CAREER). S.R.D. acknowledges the National Science Foundation for generous fellowship support. The authors would like to acknowledge Ester Kwon for critical reading of the manuscript.

REFERENCES

1. Krishnan KM, Pakhomov AB, Bao Y, Blomqvist P, Chun Y, et al. Nanomagnetism and spin electronics: materials, microstructure and novel properties. *J Mater Sci* 2006, 41(3):793–815.
2. Chemla YR, Crossman HL, Poon Y, McDermott R, Stevens R, et al. Ultrasensitive magnetic biosensor for homogeneous immunoassay. *Proc Natl Acad Sci U S A* 2000, 97(26):14268–14272.
3. Wernsdorfer W, Orozco EB, Hasselbach K, Benoit A, Barbara B, et al. Experimental evidence of the Neel-Brown model of magnetization reversal. *Phys Rev Lett* 1997, 78(9):1791–1794.
4. Connolly J, St Pierre TG. Proposed biosensors based on time-dependent properties of magnetic fluids. *J Magn Magn Mater* 2001, 225(1–2):156–160.
5. Fannin PC, Charles SW. On the calculation of the neel relaxation-time in uniaxial single-domain ferromagnetic particles. *J Phys D Appl Phys* 1994, 27(2):185–188.
6. Brown WF. Thermal fluctuations of a single-domain particle. *Phys Rev* 1963, 1(5):1677–1686.
7. Huber DL. Synthesis, properties, and applications of iron nanoparticles. *Small* 2005, 1(5):482–501.
8. Katz E, Willner I. Integrated nanoparticle-biomolecule hybrid systems: synthesis, properties, and applications. *Angew Chem Int Ed* 2004, 43(45):6042–6108.
9. Yang J, Gunn J, Dave SR, Zhang MQ, Wang YA, et al. Ultrasensitive detection and molecular imaging with magnetic nanoparticles. *Analyst* 2008, 133(2):154–160.
10. Weissleder R, Kelly K, Sun EY, Shtatland T, Josephson L. Cell-specific targeting of nanoparticles by multivalent attachment of small molecules. *Nat Biotechnol* 2005, 23(11):1418–1423.
11. Ito A, Ino K, Hayashida M, Kobayashi T, Matsunuma H, et al. Novel methodology for fabrication of tissue-engineered tubular constructs using magnetite nanoparticles and magnetic force. *Tissue Eng* 2005, 11(9–10):1553–1561.
12. Weissleder R. Molecular imaging in cancer. *Science* 2006, 312(5777):1168–1171.
13. Jurgons R, Seliger C, Hilpert A, Trahms L, Odenbach S, et al. Drug loaded magnetic nanoparticles for cancer therapy. *J Phys Condens Matter* 2006, 18(38):S2893–S2902.
14. Ito A, Shinkai M, Honda H, Kobayashi T. Medical application of functionalized magnetic nanoparticles. *J Biosci Bioeng* 2005, 100(1):1–11.
15. Johannsen M, Thiesen B, Gneveckow U, Taymoorian K, Waldofner N, et al. Thermotherapy using magnetic nanoparticles combined with external radiation in an orthotopic rat model of prostate cancer. *Prostate* 2006, 66(1):97–104.
16. Schillinger U, Brill T, Rudolph C, Huth S, Gersting S, et al. Advances in magnetofection—magnetically guided nucleic acid delivery. *J Magn Magn Mater* 2005, 293(1):501–508.
17. Simonsen CZ, Ostergaard L, Vestergaard-Poulsen P, Rohl L, Bjornerud A, et al. CBF and CBV measurements by USPIO bolus tracking: reproducibility and comparison with Gd-based values. *J Magn Reson Imaging* 1999, 9(2):342–347.
18. Kurtkoti J, Snow T, Hiremagalur B. Gadolinium and nephrogenic systemic fibrosis: association or causation. *Nephrology (Carlton)* 2008, 13(3):235–241.
19. Morcos SK. Nephrogenic systemic fibrosis following the administration of extracellular gadolinium based contrast agents: is the stability of the contrast agent molecule an important factor in the pathogenesis of this condition? *Br J Radiol* 2007, 80(950):73–76.
20. Ersoy H, Rybicki FJ. Biochemical safety profiles of gadolinium-based extracellular contrast agents and nephrogenic systemic fibrosis. *J Magn Reson Imaging* 2007, 26(5):1190–1197.
21. Thakral C, Alhariri J, Abraham JL. Long-term retention of gadolinium in tissues from nephrogenic systemic fibrosis patient after multiple gadolinium-enhanced MRI scans: case report and implications. *Constrast Media Mol Imaging* 2007, 2(4):199–205.
22. Muldoon LL, Sandor M, Pinkston KE, Neuwelt EA. Imaging, distribution, and toxicity of superparamagnetic iron oxide magnetic resonance nanoparticles in the rat brain and intracerebral tumor. *Neurosurgery* 2005, 57(4):785–796, discussion 785–96.

23. Moghimi SM, Hunter AC, Murray JC. Long-circulating and target-specific nanoparticles: theory to practice. *Pharmacol Rev* 2001, 53(2):283–318.
24. Sosnovik DE, Nahrendorf M, Weissleder R. Molecular magnetic resonance imaging in cardiovascular medicine. *Circulation* 2007, 115(15):2076–2086.
25. Choi HS, Liu W, Misra P, Tanaka E, Zimmer JP, et al. Renal clearance of quantum dots. *Nat Biotechnol* 2007, 25(10):1165–1170.
26. Murray CB, Norris DJ, Bawendi MG. Synthesis and characterization of nearly monodisperse Cde (E = S, Se, Te) semiconductor nanocrystallites. *J Am Chem Soc* 1993, 115(19):8706–8715.
27. Peng XG, Manna L, Yang WD, Wickham J, Scher E, et al. Shape control of CdSe nanocrystals. *Nature* 2000, 404(6773):59–61.
28. Puntes VF, Krishnan KM, Alivisatos AP. Colloidal nanocrystal shape and size control: the case of cobalt. *Science* 2001, 291(5511):2115–2117.
29. Park J, Lee E, Hwang NM, Kang MS, Kim SC, et al. One-nanometer-scale size-controlled synthesis of monodisperse magnetic iron oxide nanoparticles. *Angew Chem Int Ed* 2005, 44(19):2872–2877.
30. Nitin N, LaConte LEW, Zurkiya O, Hu X, Bao G. Functionalization and peptide-based delivery of magnetic nanoparticles as an intracellular MRI contrast agent. *J Biol Inorg Chem* 2004, 9(6):706–712.
31. Lee SJ, Jeong JR, Shin SC, Kim JC, Chang YH, et al. Nanoparticles of magnetic ferric oxides encapsulated with poly(D,L latide-co-glycolide) and their applications to magnetic resonance imaging contrast agent. *J Magn Magn Mater* 2004, 272–276:2432–2433.
32. Thorek DLJ, Chen A, Czupryna J, Tsourkas A. Superparamagnetic iron oxide nanoparticle probes for molecular imaging. *Ann Biomed Eng* 2006, 34(1):23–38.
33. Lopez-Quintela MA, Tojo C, Blanco MC, Rio LG, Leis JR. Microemulsion dynamics and reactions in microemulsions. *Curr Opin Colloid Interface Sci* 2004, 9(3–4):264–278.
34. Ayyub P, Multani M, Barma M, Palkar VR, Vijayaraghavan R. Size-induced structural phase-transitions and hyperfine properties of microcrystalline Fe_2O_3. *J Phys C: Solid State Phys* 1988, 21(11):2229–2245.
35. Perez JAL, Quintela MAL, Mira J, Rivas J, Charles SW. Advances in the preparation of magnetic nanoparticles by the microemulsion method. *J Phys Chem B* 1997, 101(41):8045–8047.
36. Lee Y, Lee J, Bae CJ, Park JG, Noh HJ, et al. Large-scale synthesis of uniform and crystalline magnetite nanoparticles using reverse micelles as nanoreactors under reflux conditions. *Adv Funct Mater* 2005, 15(3):503–509.
37. Sjogren CE, Johansson C, Naevestad A, Sontum PC, BrileySaebo K, et al. Crystal size and properties of superparamagnetic iron oxide (SPIO) particles. *Magn Reson Imaging* 1997, 15(1):55–67.
38. Grossman HL, Myers WR, Vreeland VJ, Bruehl R, Alper MD, et al. Detection of bacteria in suspension by using a superconducting quantum interference device. *Proc Natl Acad Sci U S A* 2004, 101(1):129–134.
39. Chung SH, Hoffmann A, Bader SD, Liu C, Kay B, et al. Biological sensors based on Brownian relaxation of magnetic nanoparticles. *Appl Phys Lett* 2004, 85(14):2971–2973.
40. Bao Y, Pakhomov AB, Krishnan KM. Brownian magnetic relaxation of water-based cobalt nanoparticle ferrofluids. *J Appl Phys* 2006, 99(8):08H107.
41. Kim KS, Park JK. Magnetic force-based multiplexed immunoassay using superparamagnetic nanoparticles in microfluidic channel. *Lab Chip* 2005, 5(6):657–664.
42. Kotitz R, Weitschies W, Trahms L, Brewer W, Semmler W. Determination of the binding reaction between avidin and biotin by relaxation measurements of magnetic nanoparticles. *J Magn Magn Mater* 1999, 194(1–3):62–68.
43. Grancharov SG, Zeng H, Sun SH, Wang SX, O'Brien S, et al. Bio-functionalization of monodisperse magnetic nanoparticles and their use as biomolecular labels in a magnetic tunnel junction based sensor. *J Phys Chem B* 2005, 109(26):13030–13035.
44. Jun YW, Huh YM, Choi JS, Lee JH, Song HT, et al. Nanoscale size effect of magnetic nanocrystals and their utilization for cancer diagnosis via magnetic resonance imaging. *J Am Chem Soc* 2005, 127(16):5732–5733.
45. Yavuz CT, Mayo JT, Yu WW, Prakash A, Falkner JC, et al. Low-field magnetic separation of monodisperse Fe_3O_4 nanocrystals. *Science* 2006, 314(5801):964–967.
46. Griffiths CH, Ohoro MP, Smith TW. Structure, magnetic characterization, and oxidation of colloidal iron dispersions. *J Appl Phys* 1979, 50(11):7108–7115.
47. Peng ZA, Peng XG. Formation of high-quality CdTe, CdSe, and CdS nanocrystals using CdO as precursor. *J Am Chem Soc* 2001, 123(1):183–184.
48. Qu LH, Peng ZA, Peng XG. Alternative routes toward high quality CdSe nanocrystals. *Nano Lett* 2001, 1(6):333–337.
49. Hines MA, Guyot-Sionnest P. Synthesis and characterization of strongly luminescing ZnS-Capped CdSe nanocrystals. *J Phys Chem* 1996, 100(2):468–471.
50. Peng XG, Schlamp MC, Kadavanich AV, Alivisatos AP. Epitaxial growth of highly luminescent CdSe/CdS core/shell nanocrystals with photostability and

electronic accessibility. *J Am Chem Soc* 1997, 119(30):7019–7029.

51. Dabbousi BO, RodriguezViejo J, Mikulec FV, Heine JR, Mattoussi H, et al. (CdSe)ZnS core-shell quantum dots: synthesis and characterization of a size series of highly luminescent nanocrystallites. *J Phys Chem B* 1997, 101(46):9463–9475.
52. Rockenberger J, Scher EC, Alivisatos AP. A new nonhydrolytic single-precursor approach to surfactant-capped nanocrystals of transition metal oxides. *J Am Chem Soc* 1999, 121(49):11595–11596.
53. Hyeon T, Lee SS, Park J, Chung Y, Bin Na H. Synthesis of highly crystalline and monodisperse maghemite nanocrystallites without a size-selection process. *J Am Chem Soc* 2001, 123(51):12798–12801.
54. Park J, An KJ, Hwang YS, Park JG, Noh HJ, et al. Ultra-large-scale syntheses of monodisperse nanocrystals. *Nat Mater* 2004, 3(12):891–895.
55. Jana NR, Chen YF, Peng XG. Size- and shape-controlled magnetic (Cr, Mn, Fe, Co, Ni) oxide nanocrystals via a simple and general approach. *Chem Mater* 2004, 16(20):3931–3935.
56. Sun SH, Murray CB, Weller D, Folks L, Moser A. Monodisperse FePt nanoparticles and ferromagnetic FePt nanocrystal superlattices. *Science* 2000, 287(5460):1989–1992.
57. Chen M, Liu JP, Sun SH. One-step synthesis of FePt nanoparticles with tunable size. *J Am Chem Soc* 2004, 126(27):8394–8395.
58. Sun SH, Zeng H, Robinson DB, Raoux S, Rice PM, et al. Monodisperse MFe2O4 (M = Fe, Co, Mn) nanoparticles. *J Am Chem Soc* 2004, 126(1):273–279.
59. Weissleder R, Mahmood U. Molecular imaging. *Radiology* 2001, 219(2):316–333.
60. Rudin M, Weissleder R. Molecular imaging in drug discovery and development. *Nat Rev Drug Discov* 2003, 2(2):123–131.
61. Gu HW, Zheng RK, Zhang XX, Xu B. Facile one-pot synthesis of bifunctional heterodimers of nanoparticles: a conjugate of quantum dot and magnetic nanoparticles. *J Am Chem Soc* 2004, 126(18):5664–5665.
62. Jun YW, Choi JS, Cheon J. Shape control of semiconductor and metal oxide nanocrystals through nonhydrolytic colloidal routes. *Angew Chem Int Ed* 2006, 45(21):3414–3439.
63. Nunez NO, Tartaj P, Morales P, Pozas R, Ocana M, et al. Preparation, characterization, and magnetic properties of Fe-based alloy particles with elongated morphology. *Chem Mater* 2003, 15(18):3558–3563.
64. Park SJ, Kim S, Lee S, Khim ZG, Char K, et al. Synthesis and magnetic studies of uniform iron nanorods and nanospheres. *J Am Chem Soc* 2000, 122(35):8581–8582.
65. Dumestre F, Chaudret B, Amiens C, Fromen MC, Casanove MJ, et al. Shape control of thermodynamically stable cobalt nanorods through organometallic chemistry. *Angew Chem Int Ed* 2002, 41(22):4286–4289.
66. Dumestre F, Chaudret B, Amiens C, Renaud P, Fejes P. Superlattices of iron nanocubes synthesized from $Fe[N(SiMe_3)(2)]_{(2)}$. *Science* 2004, 303(5659):821–823.
67. Piao Y, Kim J, Bin Na H, Kim D, Baek JS, et al. Wrap-bake-peel process for nanostructural transformation from beta-FeOOH nanorods to biocompatible iron oxide nanocapsules. *Nat Mater* 2008, 7(3):242–247.
68. Liu C, Wu XW, Klemmer T, Shukla N, Weller D. Reduction of sintering during annealing of FePt nanoparticles coated with iron oxide. *Chem Mater* 2005, 17(3):620–625.
69. Park JI, Cheon J. Synthesis of "solid solution" and "core-shell" type cobalt-platinum magnetic nanoparticles via transmetalation reactions. *J Am Chem Soc* 2001, 123(24):5743–5746.
70. Lu AH, Salabas EL, Schuth F. Magnetic nanoparticles: Synthesis, protection, functionalization, and application. *Angew Chem Int Ed* 2007, 46(8):1222–1244.
71. Mikhaylova M, Kim DK, Bobrysheva N, Osmolowsky M, Semenov V, et al. Superparamagnetism of magnetite nanoparticles: dependence on surface modification. *Langmuir* 2004, 20(6):2472–2477.
72. Kim J, Park S, Lee JE, Jin SM, Lee JH, et al. Designed fabrication of multifunctional magnetic gold nanoshells and their application to magnetic resonance imaging and photothermal therapy. *Angew Chem Int Ed* 2006, 45(46):7754–7758.
73. Wang LY, Bai JW, Li YJ, Huang Y. Multifunctional nanoparticles displaying magnetization and near-IR absorption. *Angew Chem Int Ed* 2008, 47(13):2439–2442.
74. Green M. Organometallic based strategies for metal nanocrystal synthesis. *Chem Commun* 2005, 24:3002–3011.
75. Jeong U, Teng XW, Wang Y, Yang H, Xia YN. Superparamagnetic colloids: Controlled synthesis and niche applications. *Adv Mater* 2007, 19(1):33–60.
76. Hyeon, T. Chemical synthesis of magnetic nanoparticles. *Chem Commun* 2003, 8:927–934.
77. Casula MF, Jun YW, Zaziski DJ, Chan EM, Corrias A, et al. The concept of delayed nucleation in nanocrystal growth demonstrated for the case of iron oxide nanodisks. *J Am Chem Soc* 2006, 128(5):1675–1682.
78. Kwon SG, Piao Y, Park J, Angappane S, Jo Y, et al. Kinetics of monodisperse iron oxide nanocrystal formation by "heating-up" process. *J Am Chem Soc* 2007, 129(41):12571–12584.
79. Gupta AK, Naregalkar RR, Vaidya VD, Gupta M. Recent advances on surface engineering of magnetic

iron oxide nanoparticles and their biomedical applications. *Nanomedicine* 2007, 2(1):23–39.

80. Wu XY, Liu HJ, Liu JQ, Haley KN, Treadway JA, et al. Immunofluorescent labeling of cancer marker Her2 and other cellular targets with semiconductor quantum dots. *Nat Biotechnol* 2003, 21(1):41–46.
81. Dubertret B, Skourides P, Norris DJ, Noireaux V, Brivanlou AH, et al. *In vivo* imaging of quantum dots encapsulated in phospholipid micelles. *Science* 2002, 298(5599):1759–1762.
82. Gao XH, Cui YY, Levenson RM, Chung LWK, Nie SM. *In vivo* cancer targeting and imaging with semiconductor quantum dots. *Nat Biotechnol* 2004, 22(8):969–976.
83. Pellegrino T, Manna L, Kudera S, Liedl T, Koktysh D, et al. Hydrophobic nanocrystals coated with an amphiphilic polymer shell: a general route to water soluble nanocrystals. *Nano Lett* 2004, 4(4):703–707.
84. Murthy N, Robichaud JR, Tirrell DA, Stayton PS, Hoffman AS. The design and synthesis of polymers for eukaryotic membrane disruption. *J Controlled Release* 1999, 61(1–2):137–143.
85. Sun EY, Josephson L, Weissleder R. ''Clickable'' nanoparticles for targeted imaging. *Mol Imaging* 2006, 5(2):122–128.
86. White MA, Johnson JA, Koberstein JT, Turro NJ. Toward the syntheses of universal ligands for metal oxide surfaces: controlling surface functionality through click chemistry. *J Am Chem Soc* 2006, 128(35):11356–11357.
87. Philipse AP, Vanbruggen MPB, Pathmamanoharan C. Magnetic silica dispersions—preparation and stability of surface-modified silica particles with a magnetic core. *Langmuir* 1994, 10(1):92–99.
88. Caruso F. Nanoengineering of particle surfaces. *Adv Mater* 2001, 13(1):11–22.
89. Stober W, Fink A, Bohn E. Controlled growth of monodisperse silica spheres in micron size range. *J Colloid Interface Sci* 1968, 26(1):62–69.
90. Lu Y, Yin YD, Mayers BT, Xia YN. Modifying the surface properties of superparamagnetic iron oxide nanoparticles through a sol-gel approach. *Nano Lett* 2002, 2(3):183–186.
91. Vestal CR, Zhang ZJ. Synthesis and magnetic characterization of Mn and Co spinel ferrite-silica nanoparticles with tunable magnetic core. *Nano Lett* 2003, 3(12):1739–1743.
92. Yi DK, Selvan ST, Lee SS, Papaefthymiou GC, Kundaliya D, et al. Silica-coated nanocomposites of magnetic nanoparticles and quantum dots. *J Am Chem Soc* 2005, 127(14):4990–4991.
93. Yi DK, Lee SS, Papaefthymiou GC, Ying JY. Nanoparticle architectures templated by SiO_2/Fe_2O_3 nanocomposites. *Chem Mater* 2006, 18(3):614–619.
94. Kim J, Lee JE, Lee J, Yu JH, Kim BC, et al. Magnetic fluorescent delivery vehicle using uniform mesoporous silica spheres embedded with monodisperse magnetic and semiconductor nanocrystals. *J Am Chem Soc* 2006, 128(3):688–689.
95. Lee J, Lee Y, Youn JK, Bin Na H, Yu T, et al. Simple synthesis of functionalized superparamagnetic magnetite/silica core/shell nanoparticles and their application as magnetically separable high-performance biocatalysts. *Small* 2008, 4(1):143–152.
96. Yoon TJ, Yu KN, Kim E, Kim JS, Kim BG, et al. Specific targeting, cell sorting, and bioimaging with smart magnetic silica core-shell nanomateriats. *Small* 2006, 2(2):209–215.
97. Yoon TJ, Kim JS, Kim BG, Yu KN, Cho MH, et al. Multifunctional nanoparticles possessing a ''magnetic motor effect'' for drug or gene delivery. *Angew Chem Int Ed* 2005, 44(7):1068–1071.
98. Wang LY, Luo J, Fan Q, Suzuki M, Suzuki IS, et al. Monodispersed core-shell Fe_3O_4@Au nanoparticles. *J Phys Chem B* 2005, 109(46):21593–21601.
99. Wang LY, Luo J, Maye MM, Fan Q, Qiang RD, et al. Iron oxide-gold core-shell nanoparticles and thin film assembly. *J Mater Chem* 2005, 15(18):1821–1832.
100. Caruntu D, Cushing BL, Caruntu G, O'Connor CJ. Attachment of gold nanograins onto colloidal magnetite nanocrystals. *Chem Mater* 2005, 17(13):3398–3402.
101. Lyon JL, Fleming DA, Stone MB, Schiffer P, Williams ME. Synthesis of Fe oxide core/Au shell nanoparticles by iterative hydroxylamine seeding. *Nano Lett* 2004, 4(4):719–723.
102. Mandal M, Kundu S, Ghosh SK, Panigrahi S, Sau TK, et al. Magnetite nanoparticles with tunable gold or silver shell. *J Colloid Interface Sci* 2005, 286(1):187–194.
103. Lin J, Zhou WL, Kumbhar A, Wiemann J, Fang JY, et al. Gold-coated iron (Fe@Au) nanoparticles: synthesis, characterization, and magnetic field-induced self-assembly. *J Solid State Chem* 2001, 159(1):26–31.
104. Ban ZH, Barnakov YA, Golub VO, O'Connor CJ. The synthesis of core-shell iron@gold nanoparticles and their characterization. *J Mater Chem* 2005, 15(43):4660–4662.
105. Lim J, Eggeman A, Lanni F, Tilton RD, Majetich SA. Synthesis and single-particle optical detection of low-polydispersity plasmonic-superparamagnetic nanoparticles. *Adv Mater* 2008, 20(9):1721–1726.
106. Hirsch LR, Gobin AM, Lowery AR, Tam F, Drezek RA, et al. Metal nanoshells. *Ann Biomed Eng* 2006, 34(1):15–22.
107. Artemov D, Mori N, Okollie B, Bhujwalla ZM. MR molecular imaging of the Her-2/neu receptor in breast

cancer cells using targeted iron oxide nanoparticles. *Magn Reson Med* 2003, 49(3):403–408.

108. Goldman ER, Medintz IL, Mattoussi H. Luminescent quantum dots in immunoassays. *Anal Bioanal Chem* 2006, 384(3):560–563.
109. Hermanson GT, *Bioconjugate Techniques*. San Diego: Academic Press, 1996.
110. Kumar S, Aaron J, Sokolov K. Directional conjugation of antibodies to nanoparticles for synthesis of multiplexed optical contrast agents with both delivery and targeting moieties. *Nat Protoc* 2008, 3(2):314–320.
111. Lin CAJ, Sperling RA, Li JK, Yang TY, Li PY, et al. Design of an amphiphilic polymer for nanoparticle coating and functionalization. *Small* 2008, 4(3):334–341.
112. Perez JM, Josephson L, Weissleder R. Use of magnetic nanoparticles as nanosensors to probe for molecular interactions. *Chembiochem* 2004, 5(3):261–264.
113. Josephson L, Perez JM, Weissleder R. Magnetic nanosensors for the detection of oligonucleotide sequences. *Angew Chem Int Ed* 2001, 40(17):3204–3206.
114. Perez JM, Josephson L, O'Loughlin T, Hogemann D, Weissleder R. Magnetic relaxation switches capable of sensing molecular interactions. *Nat Biotechnol* 2002, 20(8):816–820.
115. Grimm J, Perez JM, Josephson L, Weissleder R. Novel nanosensors for rapid analysis of telomerase activity. *Cancer Res* 2004, 64(2):639–643.
116. Tsourkas A, Hofstetter O, Hofstetter H, Weissleder R, Josephson L. Magnetic relaxation switch immunosensors detect enantiomeric impurities. *Angew Chem Int Ed* 2004, 43(18):2395–2399.
117. Sun EY, Weissleder R, Josephson L. Continuous analyte sensing with magnetic nanoswitches. *Small* 2006, 2(10):1144–1147.
118. Perez JM, Simeone FJ, Saeki Y, Josephson L, Weissleder R. Viral-induced self-assembly of magnetic nanoparticles allows the detection of viral particles in biological media. *J Am Chem Soc* 2003, 125(34):10192–10193.
119. Perez JM, O'Loughin T, Simeone FJ, Weissleder R, Josephson L. DNA-based magnetic nanoparticle assembly acts as a magnetic relaxation nanoswitch allowing screening of DNA-cleaving agents. *J Am Chem Soc* 2002, 124(12):2856–2857.
120. Perez JM, Simeone FJ, Tsourkas A, Josephson L, Weissleder R. Peroxidase substrate nanosensors for MR imaging. *Nano Lett* 2004, 4(1):119–122.
121. Sun EY, Josephson L, Kelly KA, Weissleder R. Development of nanoparticle libraries for biosensing. *Bioconjug Chem* 2006, 17(1):109–113.
122. Sathe TR, Agrawal A, Nie SM. Mesoporous silica beads embedded with semiconductor quantum dots and iron oxide nanocrystals: Dual-function microcarriers for optical encoding and magnetic separation. *Anal Chem* 2006, 78(16):5627–5632.
123. Insin N, Tracy JB, Lee H, Zimmer JP, Westervelt RM, et al. Incorporation of iron oxide nanoplarticles and quantum dots into silica microspheres. *ACS Nano* 2008, 2(2):197–202.
124. Su XL, Li YB. Quantum dot biolabeling coupled with immunomagnetic separation for detection of Escherichia coli O157: H7. *Anal Chem* 2004, 76(16):4806–4810.
125. Nam JM, Wise AR, Groves JT. Colorimetric bio-barcode amplification assay for cytokines. *Anal Chem* 2005, 77(21):6985–6988.
126. Nam JM, Jang KJ, Groves JT. Detection of proteins using a colorimetric bio-barcode assay. *Nat Protoc* 2007, 2(6):1438–1444.
127. Oh BK, Nam JM, Lee SW, Mirkin CA. A fluorophore-based bio-barcode amplification assay for proteins. *Small* 2006, 2(1):103–108.
128. Squires TM, Messinger RJ, Manalis SR. Making it stick: convection, reaction and diffusion in surface-based biosensors. *Nat Biotechnol* 2008, 26(4):417–426.
129. Mornet S, Vasseur S, Grasset F, Duguet E. Magnetic nanoparticle design for medical diagnosis and therapy. *J Mater Chem* 2004, 14(14):2161–2175.
130. Lee JH, Huh YM, Jun Y, Seo J, Jang J, et al. Artificially engineered magnetic nanoparticles for ultra-sensitive molecular imaging. *Nat Med* 2007, 13(1):95–99.
131. Seo WS, Lee JH, Sun XM, Suzuki Y, Mann D, et al. FeCo/graphitic-shell nanocrystals as advanced magnetic-resonance-imaging and near-infrared agents. *Nat Mater* 2006, 5(12):971–976.
132. Sasaki M, Shibata E, Kanbara Y, Ehara S. Enhancement effects and relaxivities of gadolinium-DTPA at 1.5 versus 3 Tesla: a phantom study. *Magn Reson Med Sci* 2005, 4(3):145–149.
133. Na HB, Lee JH, An KJ, Park YI, Park M, et al. Development of a T-1 contrast agent for magnetic resonance imaging using MnO nanoparticles. *Angew Chem Int Ed* 2007, 46(28):5397–5401.
134. Schick F. Whole-body MRI at high field: technical limits and clinical potential. *Eur Radiol* 2005, 15(5):946–959.
135. Hogemann D, Josephson L, Weissleder R, Basilion JP. Improvement of MRI probes to allow efficient detection of gene expression. *Bioconjug Chem* 2000, 11(6):941–946.
136. Weissleder R, Moore A, Mahmood U, Bhorade R, Benveniste H, et al. *In vivo* magnetic resonance imaging of transgene expression. *Nat Med* 2000, 6(3):351–355.

137. Sudimack J, Lee RJ. Targeted drug delivery via the folate receptor. *Adv Drug Deliv Rev* 2000, 41(2):147–162.

138. Choi H, Choi SR, Zhou R, Kung HF, Chen IW. Iron oxide nanoparticles as magnetic resonance contrast agent for tumor imaging via folate receptor-targeted delivery. *Acad Radiol* 2004, 11(9):996–1004.

139. Sosnovik DE, Schellenberger EA, Nahrendorf M, Novikov MS, Matsui T, et al. Magnetic resonance imaging of cardiomyocyte apoptosis with a novel magneto-optical nanoparticle. *Magn Reson Med* 2005, 54(3):718–724.

140. Schellenberger EA, Hogemann D, Josephson L, Weissleder R. Annexin V-CLIO: a nanoparticle for detecting apoptosis by MRI. *Acad Radiol* 2002, 9:S310–S311.

141. Kelly KA, Allport JR, Tsourkas A, Shinde-Patil VR, Josephson L, et al. Detection of vascular adhesion molecule-1 expression using a novel multimodal nanoparticle. *Circ Res* 2005, 96(3):327–336.

142. Tsourkas A, Shinde-Patil VR, Kelly KA, Patel P, Wolley A, et al. *In vivo* imaging of activated endothelium using an anti-VCAM-1 magnetooptical probe. *Bioconjug Chem* 2005, 16(3):576–581.

143. Huh YM, Jun YW, Song HT, Kim S, Choi JS, et al. *In vivo* magnetic resonance detection of cancer by using multifunctional magnetic nanocrystals. *J Am Chem Soc* 2005, 127(35):12387–12391.

144. Hultman KL, Raffo AJ, Grzenda AL, Harris PE, Brown TR, et al. Magnetic resonance imaging of major histocompatibility class II expression in the renal medulla using immunotargeted superparamagnetic iron oxide nanoparticles. *ACS Nano* 2008, 2(3):477–484.

145. Modo M, Hoehn M, Bulte JW. Cellular MR imaging. *Mol Imaging* 2005, 4(3):143–164.

146. Bulte JWM, Duncan ID, Frank JA. *In vivo* magnetic resonance tracking of magnetically labeled cells after transplantation. *J Cereb Blood Flow Metab* 2002, 22(8):899–907.

147. Kraitchman DL, Heldman AW, Atalar E, Amado LC, Martin BJ, et al. *In vivo* magnetic resonance imaging of mesenchymal stem cells in myocardial infarction. *Circulation* 2003, 107(18):2290–2293.

148. Lewin M, Carlesso N, Tung CH, Tang XW, Cory D, et al. Tat peptide-derivatized magnetic nanoparticles allow in vivo tracking and recovery of progenitor cells. *Nat Biotechnol* 2000, 18(4):410–414.

149. Bulte JWM, Douglas T, Witwer B, Zhang SC, Strable E, et al. Magnetodendrimers allow endosomal magnetic labeling and *in vivo* tracking of stem cells. *Nat Biotechnol* 2001, 19(12):1141–1147.

150. Dodd SJ, Williams M, Suhan JP, Williams DS, Koretsky AP, et al. Detection of single mammalian cells by high-resolution magnetic resonance imaging. *Biophys J* 1999, 76(1):103–109.

151. Shapiro EM, Skrtic S, Sharer K, Hill JM, Dunbar CE, et al. MRI detection of single particles for cellular imaging. *Proc Natl Acad Sci U S A* 2004, 101(30):10901–10906.

152. Shapiro EM, Skrtic S, Koretsky AP. Sizing it up: cellular MRI using micron-sized iron oxide particles. *Magn Reson Med* 2005, 53(2):329–338.

153. Shapiro EM, Sharer K, Skrtic S, Koretsky AP. *In vivo* detection of single cells by MRI. *Magn Reson Med* 2006, 55(2):242–249.

154. Hoehn M, Wiedermann D, Justicia C, Ramos-Cabrer P, Kruttwig K, et al. Cell tracking using magnetic resonance imaging. *J Physiol (London)* 2007, 584(1):25–30.

155. Saleh A, Wiedermann D, Schroeter M, Jonkmanns C, Jander S, et al. Central nervous system inflammatory response after cerebral infarction as detected by magnetic resonance imaging. *NMR Biomed* 2004, 17(4):163–169.

156. Kleinschnitz C, Bendszus T, Frank M, Solymosi T, Toyka KV, et al. *In vivo* monitoring of macrophage infiltration in experimental ischemic brain lesions by magnetic resonance imaging. *J Cereb Blood Flow Metab* 2003, 23(11):1356–1361.

157. Schroeter M, Saleh A, Wiedermann D, Hoehn M, Jander S. Histochemical detection of ultrasmall superparamagnetic iron oxide (USPIO) contrast medium uptake in experimental brain ischemia. *Magn Reson Med* 2004, 52(2):403–406.

158. Shapiro EM, Gonzalez-Perez O, Garcia-Verdugo JM, Alvarez-Buylla A, Koretsky AP. Magnetic resonance imaging of the migration of neuronal precursors generated in the adult rodent brain. *Neuroimage* 2006, 32(3):1150–1157.

159. Arbab AS, Bashaw LA, Miller BR, Jordan EK, Lewis BK, et al. Characterization of biophysical and metabolic properties of cells labeled with superparamagnetic iron oxide nanoparticles and transfection agent for cellular MR imaging. *Radiology* 2003, 229(3):838–846.

160. Kalish H, Arbab AS, Miller BR, Lewis BK, Zywicke HA, et al. Combination of transfection agents and magnetic resonance contrast agents for cellular imaging: Relationship between relaxivities, electrostatic forces, and chemical composition. *Magn Reson Med* 2003, 50(2):275–282.

161. Weissleder R, Cheng HC, Bogdanova A, Bogdanov A. Magnetically labeled cells can be detected by MR imaging. *J Magn Reson Imaging* 1997, 7(1):258–263.

162. Walczak P, Kedziorek DA, Gilad AA, Lin S, Bulte JWM. Instant MR labeling of stem cells using magnetoelectroporation. *Magn Reson Med* 2005, 54(4):769–774.

163. Frank JA, Miller BR, Arbab AS, Zywicke HA, Jordan EK, et al. Clinically applicable labeling of mammalian and stem cells by combining; Superparamagnetic iron oxides and transfection agents. *Radiology* 2003, 228(2):480–487.

164. Josephson L, Tung CH, Moore A, Weissleder R. High-efficiency intracellular magnetic labeling with novel superparamagnetic-tat peptide conjugates. *Bioconjug Chem* 1999, 10(2):186–191.

165. Arbab AS, Yocum GT, Kalish H, Jordan EK, Anderson SA, et al. Efficient magnetic cell labeling with protamine sulfate complexed to ferumoxides for cellular MRI. *Blood* 2004, 104(4):1217–1223.

166. Schoepf U, Marecos EM, Melder RJ, Jain RK, Weissleder R. Intracellular magnetic labeling of lymphocytes for *in vivo* trafficking studies. *Biotechniques* 1998, 24(4):, 642–646 648–651.

167. Wunderbaldinger P, Josephson L, Weissleder R. Tat peptide directs enhanced clearance and hepatic permeability of magnetic nanoparticles. *Bioconjug Chem* 2002, 13(2):264–268.

168. Guzman R, Uchida N, Bliss TM, He DP, Christopherson KK, et al. Long-term monitoring of transplanted human neural stem cells in developmental and pathological contexts with MRI. *Proc Natl Acad Sci U S A* 2007, 104(24):10211–10216.

169. de Vries IJM, Lesterhuis WJ, Barentsz JO, Verdijk P, van Krieken JH, et al. Magnetic resonance tracking of dendritic cells in melanoma patients for monitoring of cellular therapy. *Nat Biotechnol* 2005, 23(11):1407–1413.

170. Walczak P, Kedziorek DA, Gilad AA, Barnett BP, Bulte JWM. Applicability and limitations of MR tracking of neural stem cells with asymmetric cell division and rapid turnover: the case of the shiverer dysmyelinated mouse brain. *Magn Reson Med* 2007, 58(2):261–269.

171. Yang J, Lee CH, Park J, Seo S, Lim EK, et al. Antibody conjugated magnetic PLGA nanoparticles for diagnosis and treatment of breast cancer. *J Mater Chem* 2007, 17(26):2695–2705.

172. Lubbe AS, Alexiou C, Bergemann C. Clinical applications of magnetic drug targeting. *J Surg Res* 2001, 95(2):200–206.

173. Lubbe AS, Bergemann C, Riess H, Schriever F, Reichardt P, et al. Clinical experiences with magnetic drag targeting: a phase I study with 4'-epidoxorubicin in 14 patients with advanced solid tumors. *Cancer Res* 1996, 56(20):4686–4693.

174. Lubbe AS, Bergemann C, Brock J, McClure DG. Physiological aspects in magnetic drug-targeting. *J Magn Magn Mater* 1999, 194(1–3):149–155.

175. Wilson MW, Kerlan RK, Fidelman NA, Venook AP, LaBerge JM, et al. Hepatocellular carcinoma: regional therapy with a magnetic targeted carrier bound to doxorubicin in a dual MR imaging/conventional angiography suite—initial experience with four patients. *Radiology* 2004, 230(1):287–293.

176. Alexiou C, Arnold W, Klein RJ, Parak FG, Hulin P, et al. Locoregional cancer treatment with magnetic drug targeting. *Cancer Res* 2000, 60(23):6641–6648.

177. Nasongkla N, Bey E, Ren JM, Ai H, Khemtong C, et al. Multifunctional polymeric micelles as cancer-targeted, MRI-ultrasensitive drug delivery systems. *Nano Lett* 2006, 6(11):2427–2430.

178. Kim J, Lee JE, Lee SH, Yu JH, Lee JH, et al. Designed fabrication of a multifunctional polymer nanomedical platform for simultaneous cancer-targeted imaging and magnetically guided drug delivery. *Adv Mater* 2008, 20(3):478–483.

179. Liong M, Lu J, Kovochich M, Xia T, Ruehm SG, et al. Multifunctional inorganic nanoparticles for imaging, targeting, and drug delivery. *ACS Nano* 2008, 2(5):889–896.

180. Dobson J. Gene therapy progress and prospects: magnetic nanoparticle-based gene delivery. *Gene Ther* 2006, 13(4):283–287.

181. Mykhaylyk O, Antequera YS, Vlaskou D, Plank C. Generation of magnetic nonviral gene transfer agents and magnetofection *in vitro*. *Nat Protoc* 2007, 2(10):2391–2411.

182. Luo D, Saltzman WM. Enhancement of transfection by physical concentration of DNA at the cell surface. *Nat Biotechnol* 2000, 18(8):893–895.

183. Plank C, Schillinger U, Scherer F, Bergemann C, Remy JS, et al. The magnetofection method: using magnetic force to enhance gene delivery. *Biol Chem* 2003, 384(5):737–747.

184. Krotz F, de Wit C, Sohn HY, Zahler S, Gloe T, et al. Magnetofection—a highly efficient tool for antisense oligonucleotide delivery *in vitro* and *in vivo*. *Mol Ther* 2003, 7(5):700–710.

185. Gersting SW, Schillinger U, Lausier J, Nicklaus P, Rudolph C, et al. Gene delivery to respiratory epithelial cells by magnetofection. *J Gen Med* 2004, 6(8):913–922.

186. Krotz F, Sohn HY, Gloe T, Plank C, Pohl U. Magnetofection potentiates gene delivery to cultured endothelial cells. *J Vasc Res* 2003, 40(5):425–434.

187. Scherer F, Anton M, Schillinger U, Henkel J, Bergemann C, et al. Magnetofection: enhancing and targeting gene delivery by magnetic force *in vitro* and *in vivo*. *Gene Ther* 2002, 9(2):102–109.

188. Xenariou S, Griesenbach U, Ferrari S, Dean P, Scheule RK, et al. Using magnetic forces to enhance non-viral gene transfer to airway epithelium *in vivo*. *Gene Ther* 2006, 13(21):1545–1552.

189. Dames P, Gleich B, Flemmer A, Hajek K, Seidl N, et al. Targeted delivery of magnetic aerosol droplets to the lung. *Nat Nanotechnol* 2007, 2(8):495–499.

190. Medarova Z, Pham W, Farrar C, Petkova V, Moore A. *In vivo* imaging of siRNA delivery and silencing in tumors. *Nat Med* 2007, 13(3):372–377.

191. Moore A, Marecos E, Simonova M, Weissleder R, Bogdanov A Jr. Novel gliosarcoma cell line expressing green fluorescent protein: a model for quantitative assessment of angiogenesis. *Microvasc Res* 1998, 56(3):145–153.

192. Mannix RJ, Kumar S, Cassiola F, Montoya-Zavala M, Feinstein E, et al. Nanomagnetic actuation of receptor-mediated signal transduction. *Nat Nanotechnol* 2008, 3(1):36–40.

193. Wolf SA, Awschalom DD, Buhrman RA, Daughton JM, von Molnar S, et al. Spintronics: a spin-based electronics vision for the future. *Science* 2001, 294(5546):1488–1495.

194. Li GX, Sun SH, Wilson RJ, White RL, Pourmand N, et al. Spin valve sensors for ultrasensitive detection of superparamagnetic nanoparticles for biological applications. *Sens Actuators A Phys* 2006, 126(1): 98–106.

195. Ferrari M. Cancer nanotechnology: opportunities and challenges. *Nat Rev Cancer* 2005, 5(3): 161–171.

